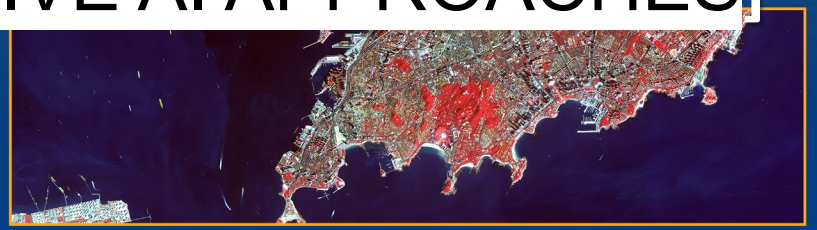
2025 DRAGON 6 SYMPOSIUM

14-18 JULY 2025

[PROJECT ID. 95407]

[ELECTROMAGNETISM ANOMALY DETECTION AND DEFORMATION MONITORING BY GENERATIVE AND PREDICTIVE AI APPROACHES]





2025 Dragon 6 Symposium

< Thursday, 17/July/2025 IN SOLID EARTH>

ID. 95407

PROJECT TITLE: ELECTROMAGNETISM ANOMALY DETECTION AND DEFORMATION MONITORING BY GENERATIVE AND PREDICTIVE AI APPROACHES

PRINCIPAL INVESTIGATORS: [PROF YAXIN BI AND PROF XUEMIN ZHANG]

CO-AUTHORS: [JIANBO SUN, MAJA PAVLOVIC, FIACHRA MERWICK, WEI ZHAI, JI TANG, JIANPING HUANG, PAN XIONG, QIAO WANG, XINYAN QUYANG]

PRESENTED BY: [PROF YAXIN BI AND PROF XUEMIN ZHANG]

Project's Objectives

- Characterise electromagnetic signals and variations of signal spectrums by features; characterise abnormal signal patterns detected from electromagnetic data, which are likely related to earthquakes
- Incorporate the Dragon 3/4/5 results into developing an advanced anomaly detection algorithm using generative AI and predictive neural networks
  - ✓ Long-Short Memory Networks (LSTM) and Reinforcement learning
  - ✓ Generative Adversarial Networks (GAN)
  - ✓ Convolution Neural Networks (CNN)
- Trace electromagnetic waves recorded before earthquakes from the lithosphere to the ionosphere.
- With the timely SAR acquisitions by Sentinel-1/2 satellites, detect seismic deformation of earthquake cycles as background knowledge
- Perform correlation analysis between anomalies and large earthquakes in depth, identify times of anomalies appearing before and during earthquakes, anomaly cycles and time duration.

Dragon 6 EO Data Delivery

Data access (list all missions and issues if any). NB. in the tables please insert cumulative figures (since June 2024) for no. of scenes of high bit rate data (e.g. S1 100 scenes). If data delivery is low bit rate by ftp, insert “ftp”

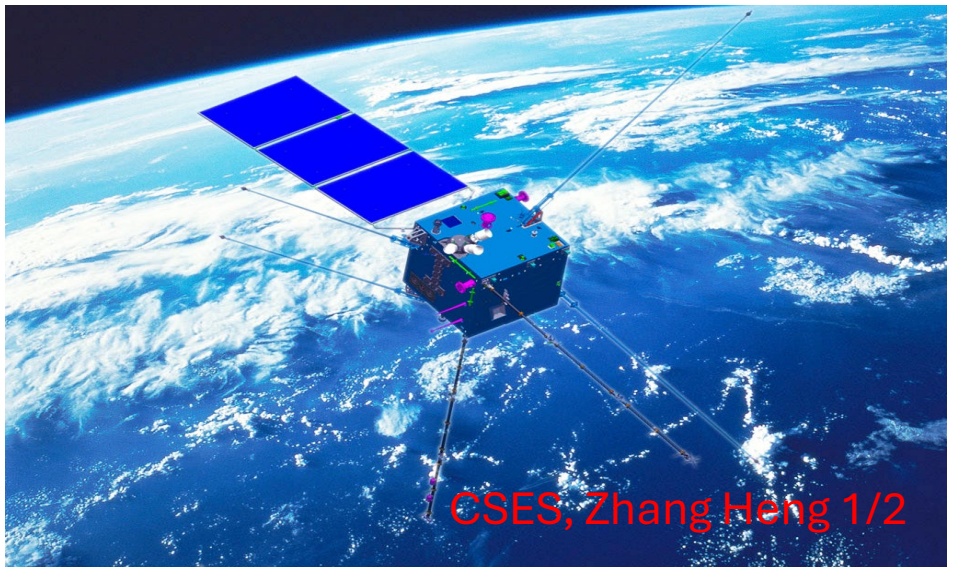
ESA /Copernicus Missions	No. Scenes
1. Swarm satellites	
2. Sentinel 1&2	
3.	
4.	
5.	
6.	
Total:	
Issues:	

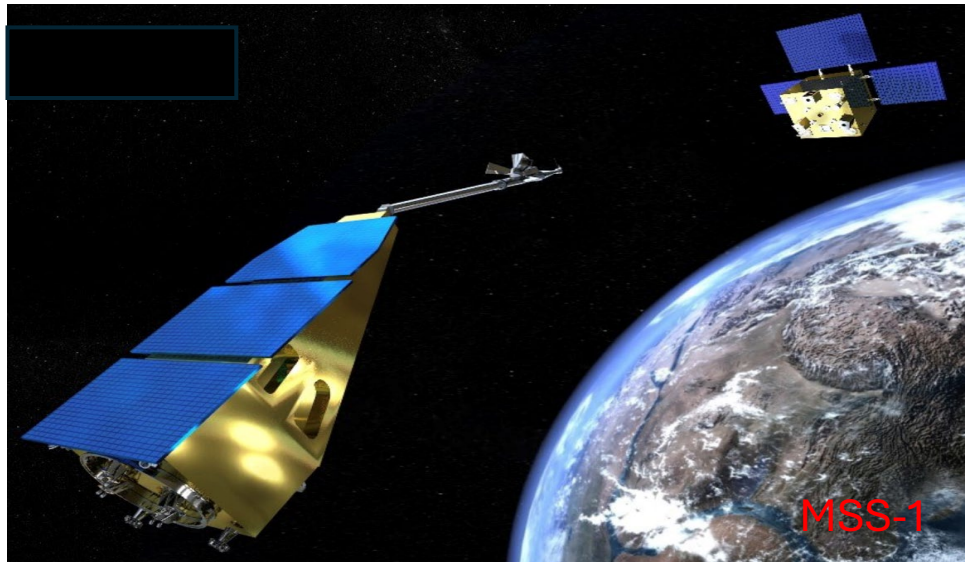
ESA Third Party Missions	No. Scenes
1.HISEA-1	
2.	
3.	
4.	
5.	
6.	
Total:	
Issues:	

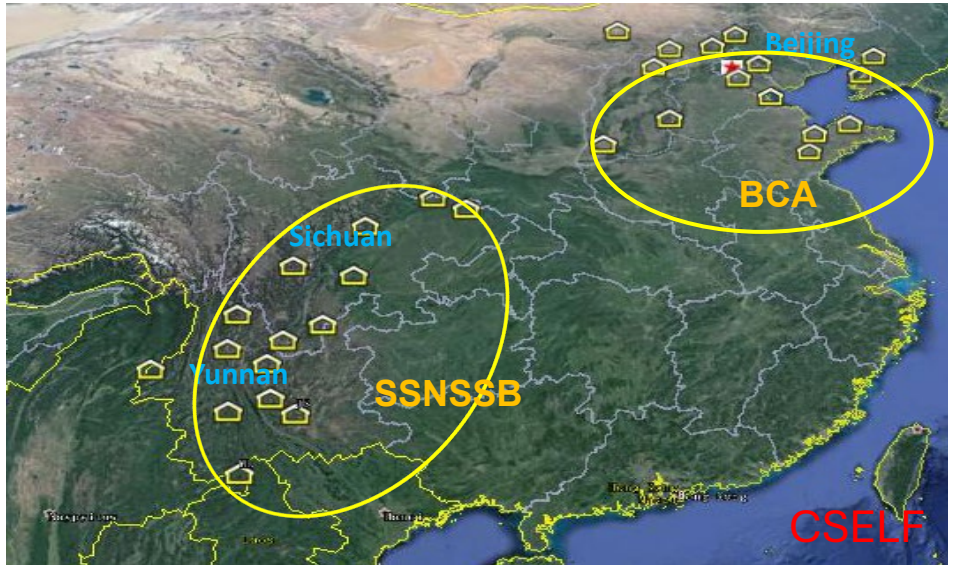
Chinese EO data	No. Scenes
1. CSES satellite 1/2	
2. CSELF network	
3. MSS-1	
4.	
5.	
6.	
Total:	
Issues:	

Data Acquisition from Four EM Sources





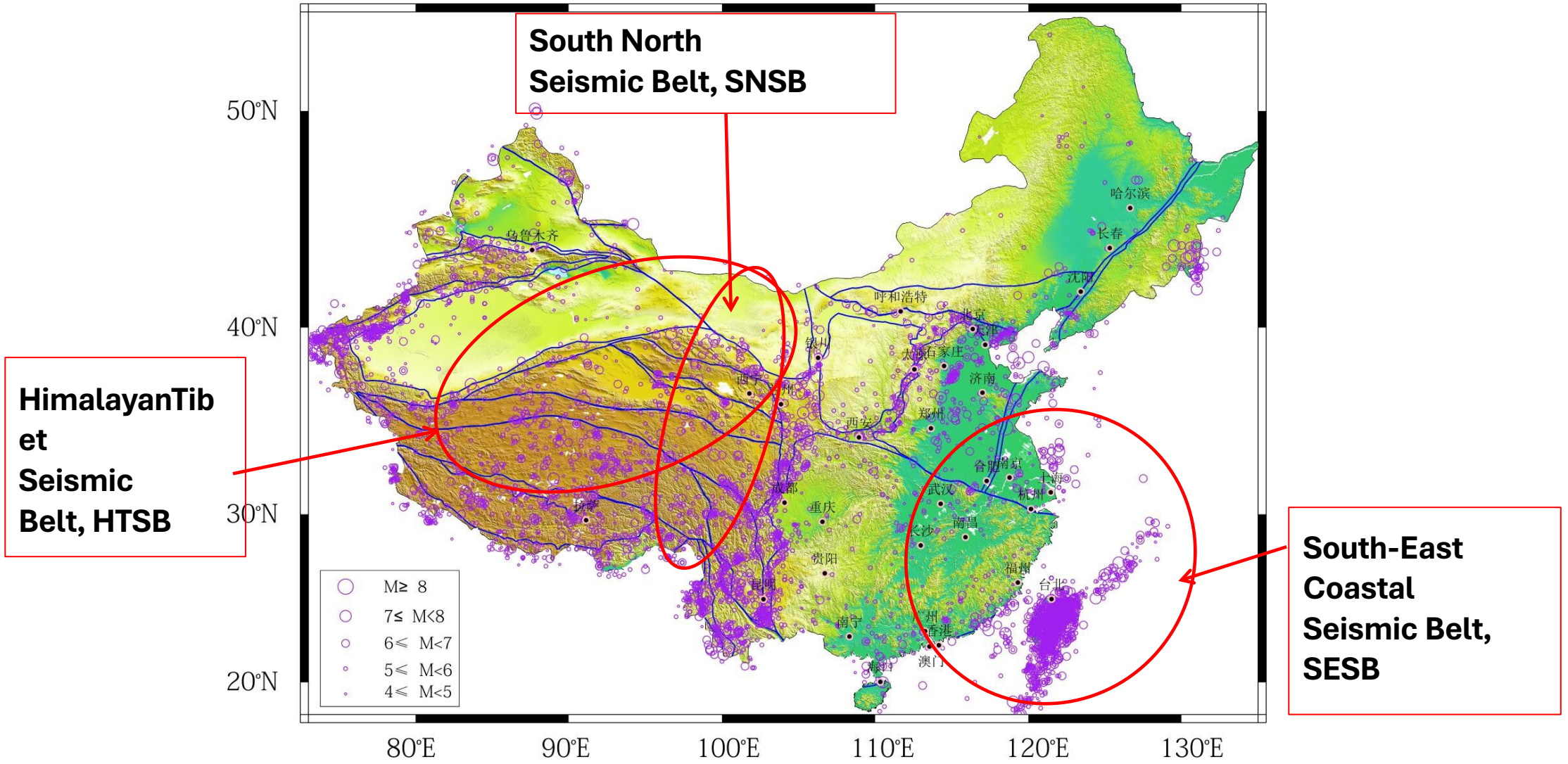




Swarm, 22/11/ 2013
CSES 1, 02/02/2018
CSES 2, 11/06/2025
Macau Science Satellites (MSS-1, 06/10/2022)

Control Source Extremely Low Frequency observation network in China (CSELF) since 2005

Three Study Areas within Seismically Active Belts



Work Packages

- WP1 Transformation of electromagnetic data
  - ✓ Transform satellite electromagnetic data into concise representations, which will be then segmented into a collection of subsequences.
- WP2 Study areas and seismic deformation of earthquake cycles
  - ✓ Use Sentinel-1 satellite data to detect the deformation of most of the shallow earthquakes happened in China and surrounding regions, which will be used in areas, such as Sichuan, Yunnan, Tibet, Xinjiang, Qinghai provinces, etc.
  - ✓ The integration of InSAR data with seismic anomalies data will provide a meaningful way to cross-examine dynamic issues of potential earthquakes in the study areas.
- WP3 Development of new detection algorithms and applications
  - ✓ Apply GAN to develop generators to generate synthetic satellite and CSELF data to tackle data sparsity problems.
  - ✓ Use LSTM and CNN to develop an innovative method for identifying anomalies
- WP4 Comparison between anomalies detected from Swarm, CESE, MSS-1 data
  - ✓ Vector Field Magnetometer (VFM): 1Hz, 50Hz, 250Hz
  - ✓ Absolute Scalar Magnetometer (ASM): 1Hz
  - ✓ Electrical Field Instrument (EFI) to measure the electron density and temperature with sampling rate of 2Hz
  - ✓ High Precision Magnetometer (HPM)
  - ✓ Langmiur Probe (LAP) to measure electron density and temperature

Work Packages (cont'd)

- WP5 Comparison on electromagnetic anomalies between CSES and CSELF
  - ✓ The CSES's instruments considered will include:
    - Search-Coil Magnetometer (SCM): band 1(10-200Hz), band 2(200-2200Hz), band 3(1.8kHz-20kHz)
    - Electric Field Detector (EFD): ULF(DC-16Hz), ELF (6Hz-2.2kHz), VLF(1.8kHz-20kHz), and HF(18kHz-3.5MHz)
  - ✓ The CSELF's instruments include:
    - CSELF at n*10^3s-n*10^3Hz - magnetic field with three components and electric field with two horizontal components

European Young Scientists contributions in Dragon 6

Name	Institution	Poster title	Contribution including period of research
Mrs Maja Pavlovic	Ulster University	Reconstructing Incomplete Geomagnetic Residuals from SWARM Satellite Data using GANs	Dragon 5 & 6
Mr Fiachra Merwick	Ulster University	n/a	Dragon 6
Mr Christopher O'Neill	Ulster University	n/a	October 2022 – September 2025

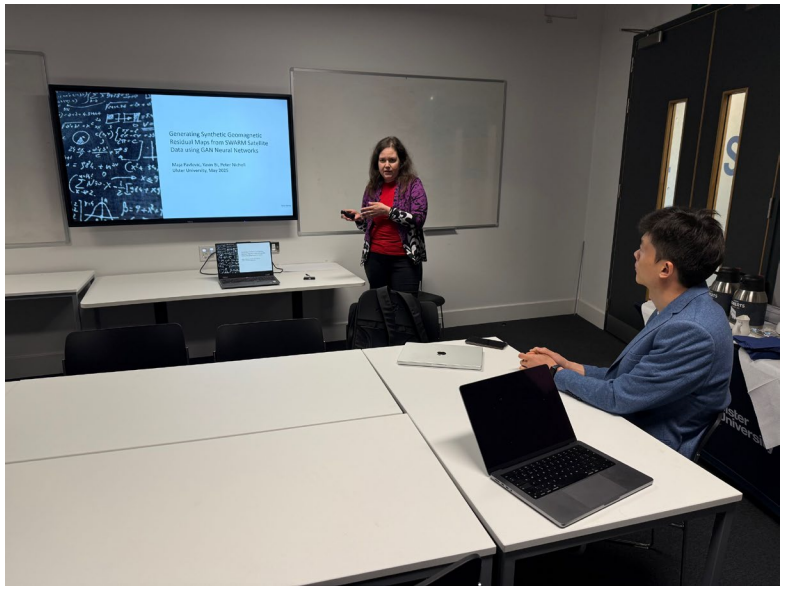
Chinese Young Scientists contributions in Dragon 6

Name	Institution	Poster title	Contribution including period of research
Mr. Haochen Wu	Institute of Earthquake Forecasting, China Earthquake Administration	n/a	Dragon 6
Miss Hong Liu	Institute of Earthquake Forecasting, China Earthquake Administration	n/a	Dragon 6
Mr. Jianghe Chen	Institute of Earthquake Forecasting, China Earthquake Administration	n/a	Dragon 6
Miss Yan Liu	Institute of Earthquake Forecasting, China Earthquake Administration	n/a	Dragon 6
Mr Shukai Wang	Institute of of Earthquake Forecasting, China Earthquake Administration	n/a	Dragon 6

Training Plan for Young Scientists

- The supervision of postgraduate students (PhD and MSc) is an essential part of training new scientists in these areas
- Provide short courses for the young scientists and members of the Dragon 6 program
- Provision of summer schools and postgraduate courses
- Encourage youths to devote their efforts to participate in research activities, and present their research findings in workshops and conferences in addition to Dragon's symposiums.
- Support mutual exchange studies and field trips

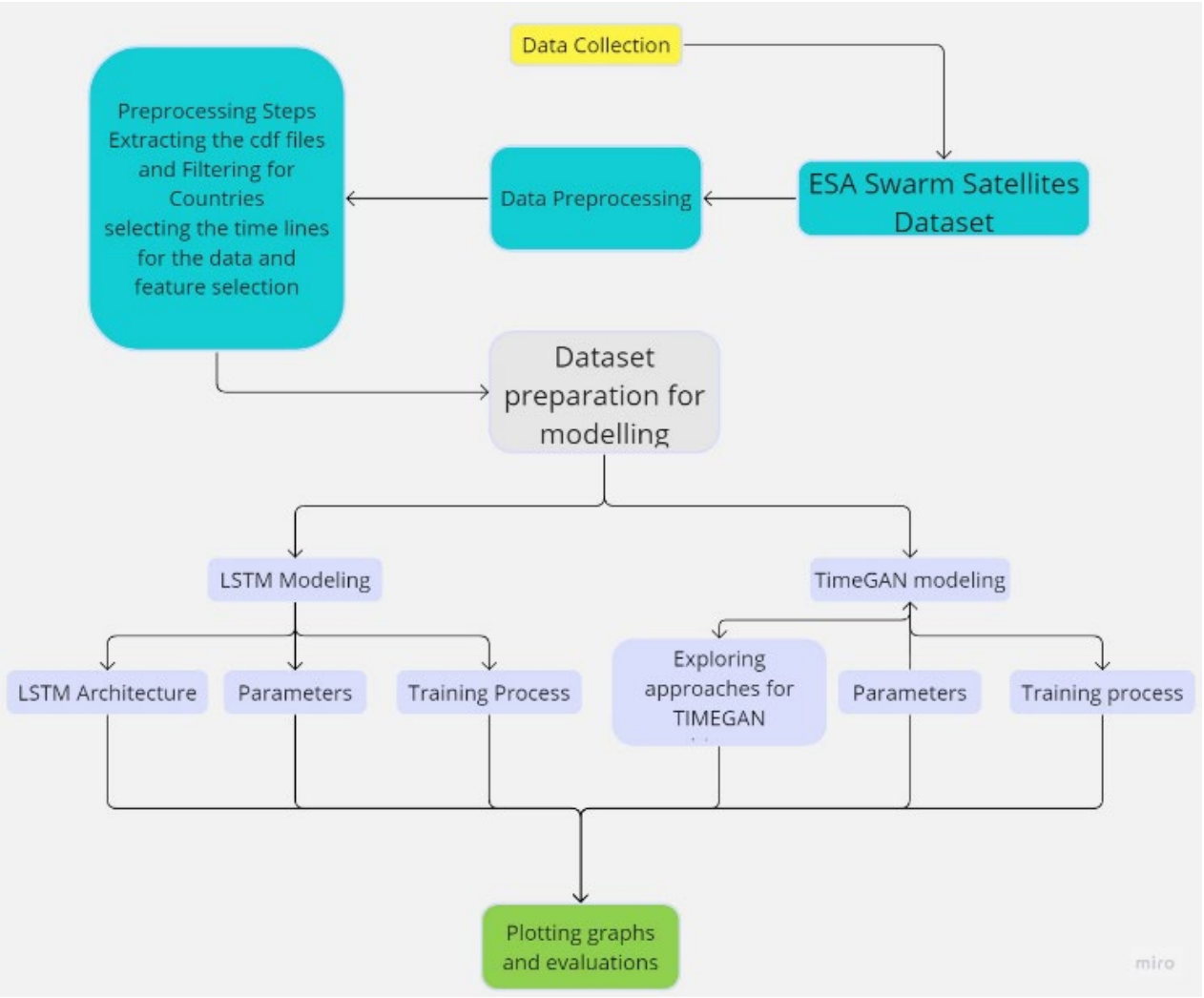
Overview of YSs Research Exchange

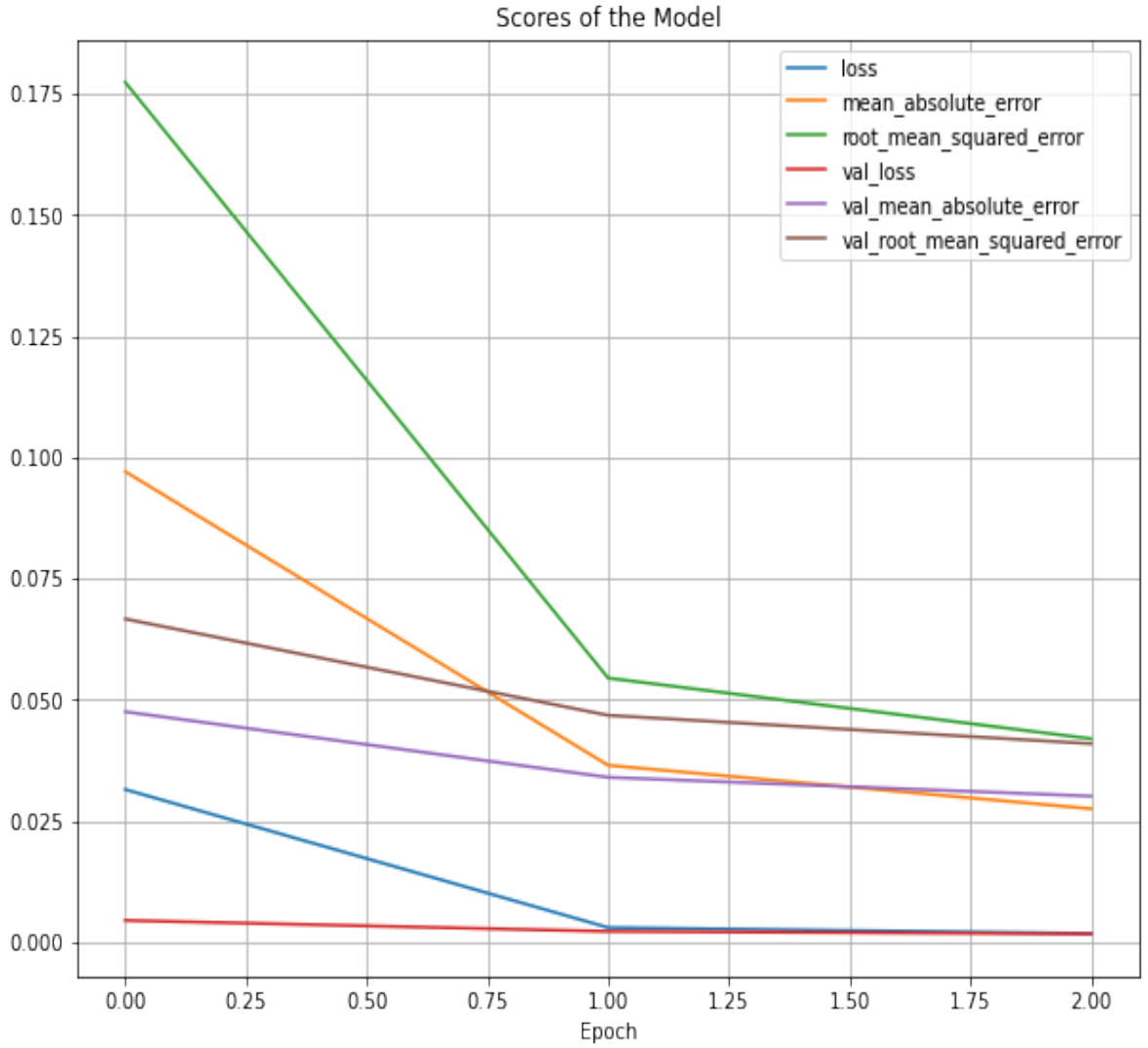






Part 1: Research Methodology
LSTM for Predicting and GAN for Generating Satellite Data

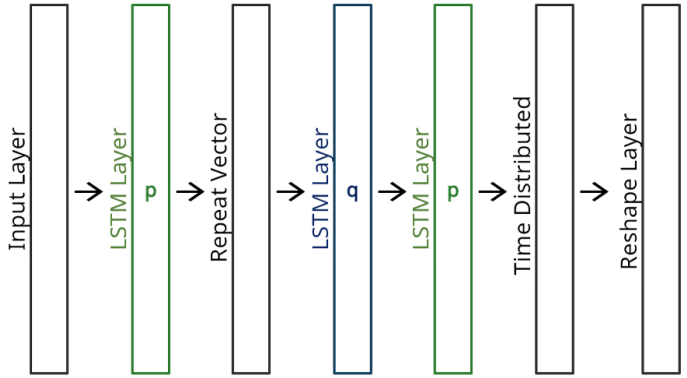


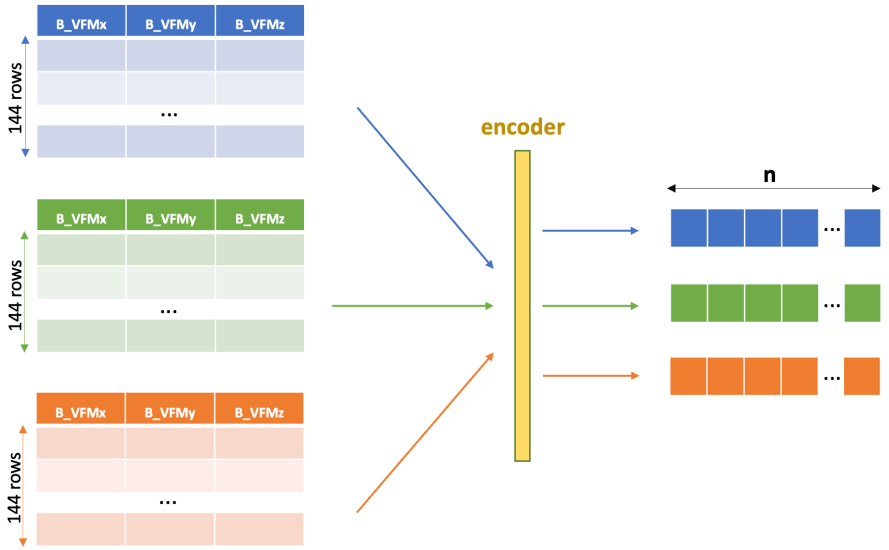


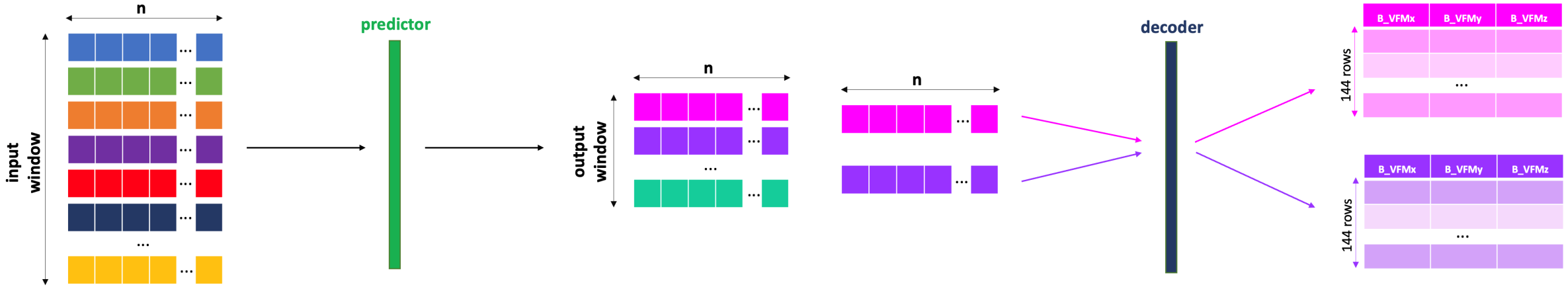
LSTM and Encoder-Predictor-Decoder

Specification

- Three LSTM layers with *p*, *q* and *p* number of neurons respectively.
- Repeat Vector, Time Distributed and Reshape layers to adjust the shape of data.
- Activation function: *tanh* with *glorot uniform* kernel initialiser.
- Error metrics: Mean Squared Error (MSE), Mean Absolute Error (MAE), Root Mean Squared Error (RMSE).







Prediction Time Frames

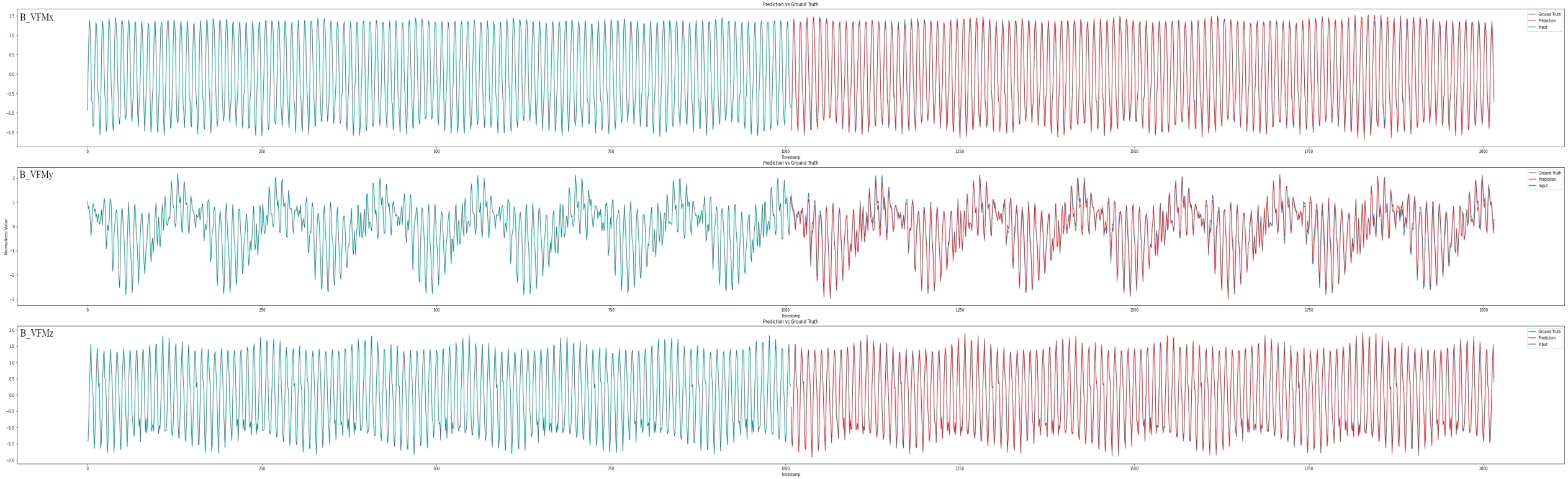
TABLE I: I/O lengths of the windows tested for the predictors

Target	Input A	Input B	Input C	Input D	Output
1 week	7	21	30	-	**7**
1 month	7	30	60	-	**30**
6 months	30	90	120	180	**180**
8 months	180	320	-	-	**240**

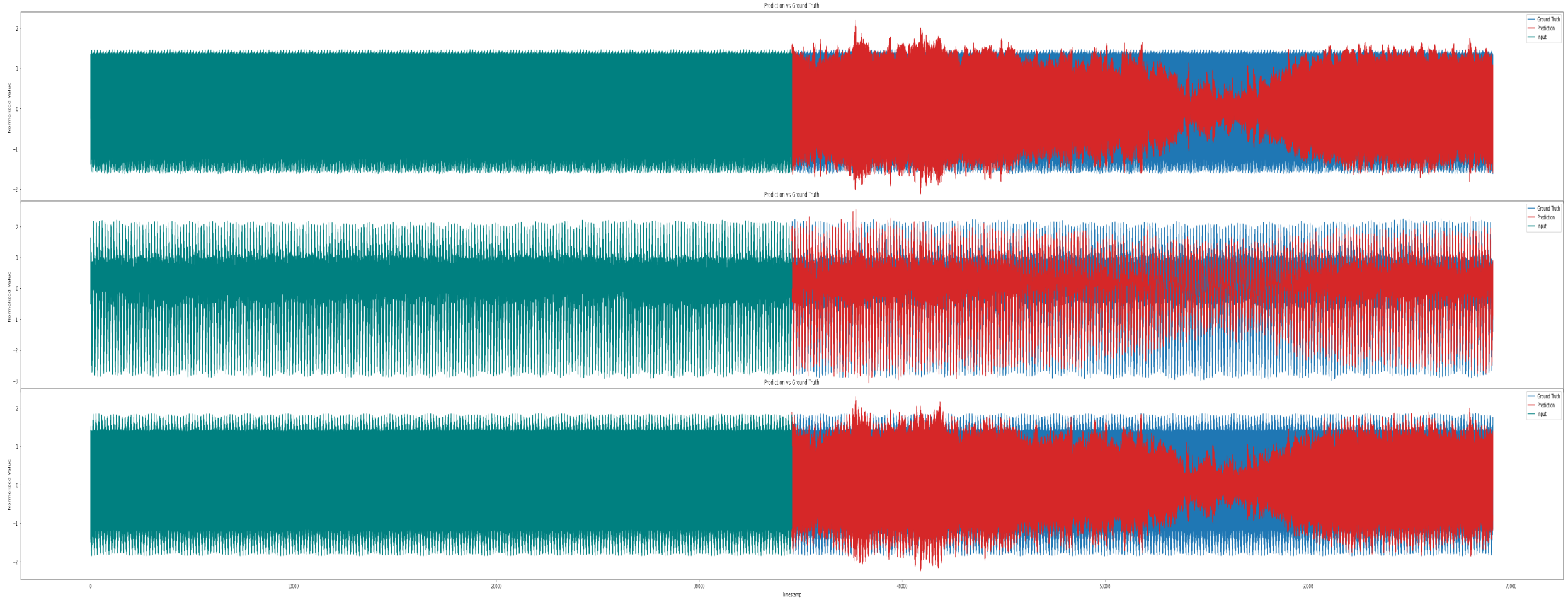
days

For our analysis, we gather all available MAGx LR packages between January 2014 and July 2021. As we acquire measurements recorded by Swarm A. All the mentioned packages belong to the Level 1B product

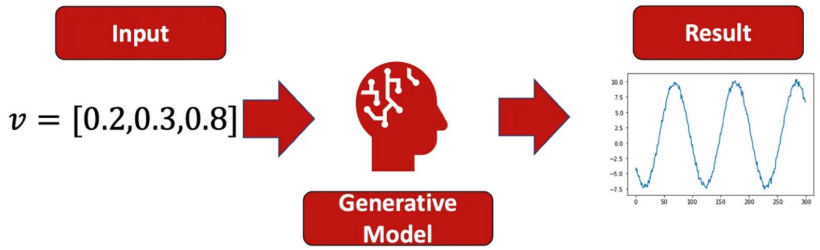
Prediction: 7 days -> 7 days

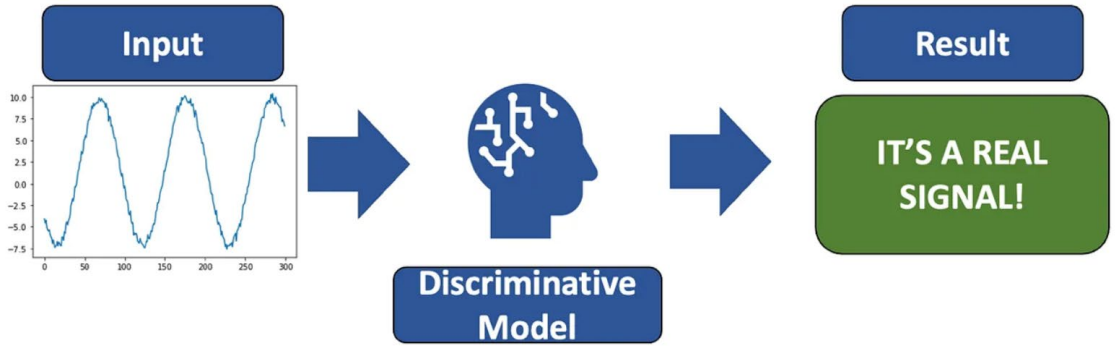


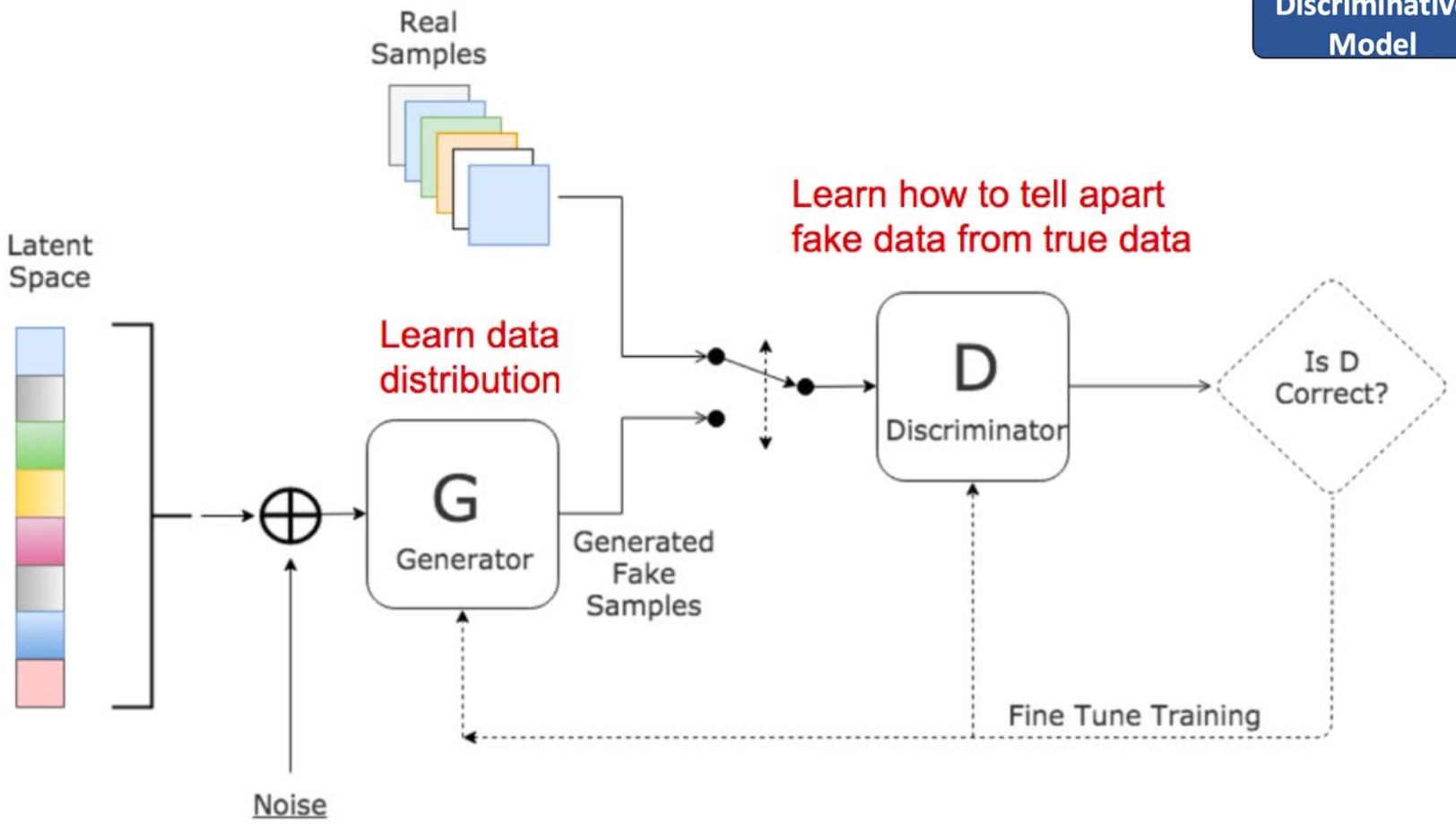
Prediction: 8 months -> 8 months



Part 2: Research Methodology - Architecture of a Generative Adversarial Network (GAN)





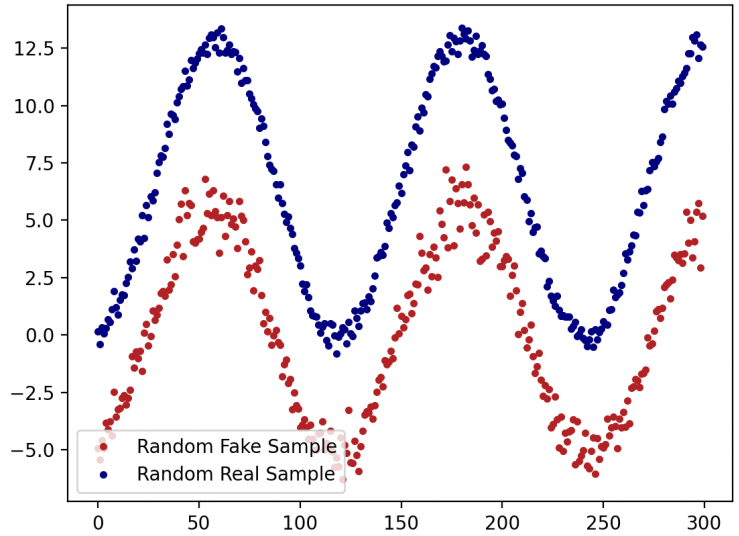


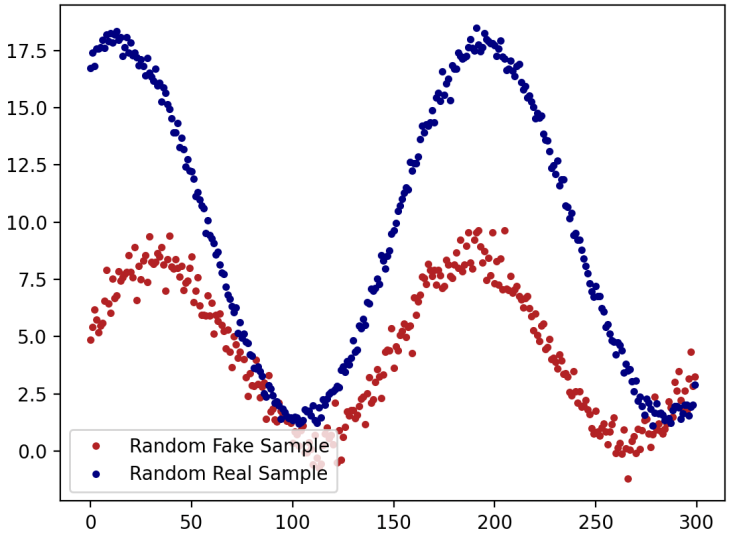
https://www.kdnuggets.com/2017/01/generative-adversarial-networks-hot-topic-machine-learning.html.

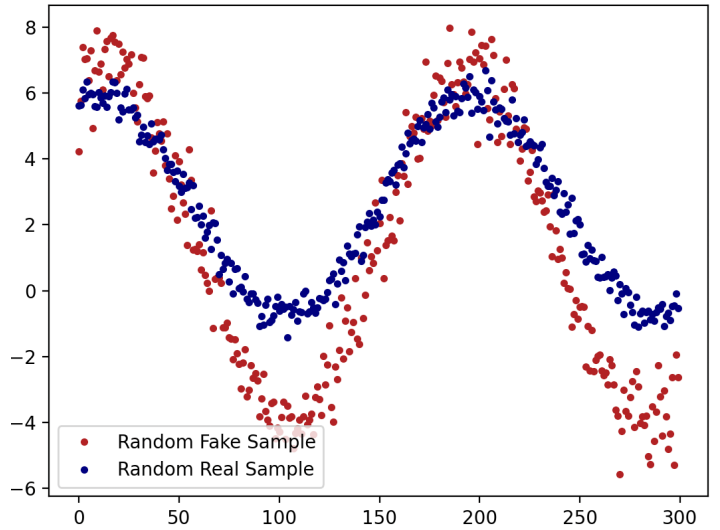
Theoretical Framework and Gradient Calculation

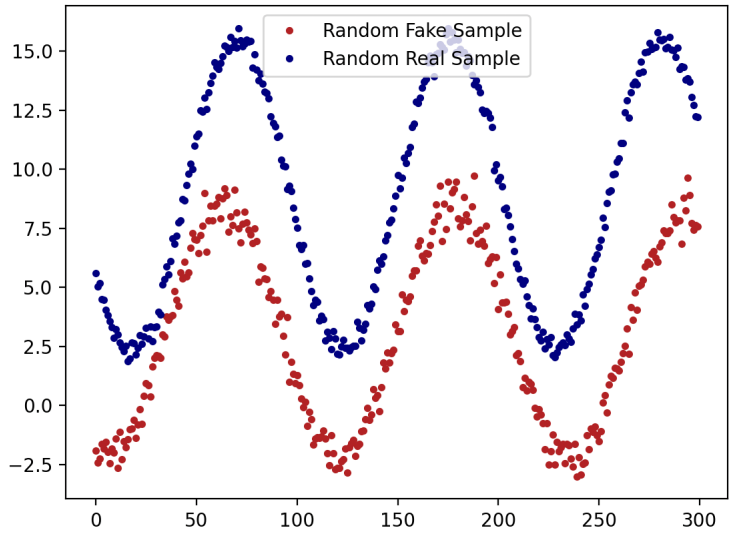
Jinsung Yoon, Daniel Jarrett, Mihaela van der Schaar. Time-series Generative Adversarial Networks, NeurIPS, 2019.

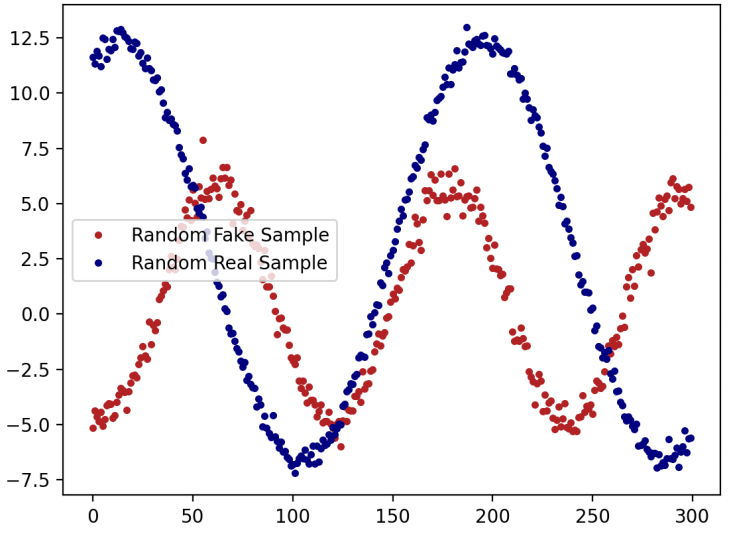
Simulated Results of a Sine Function

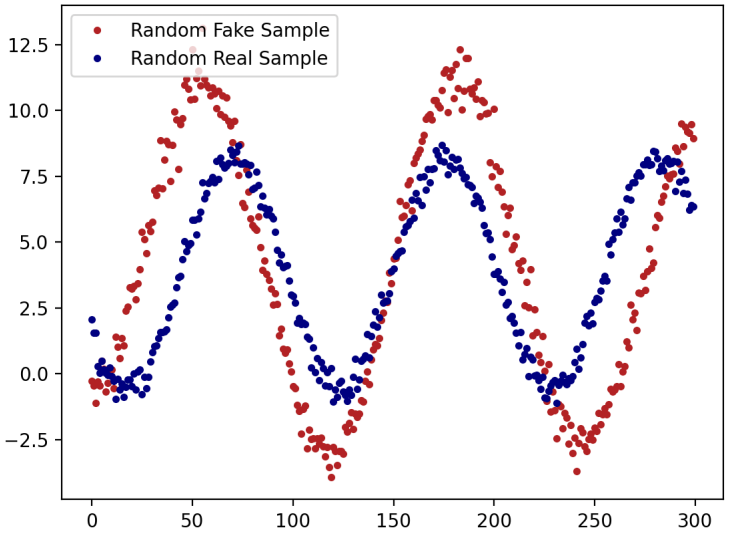




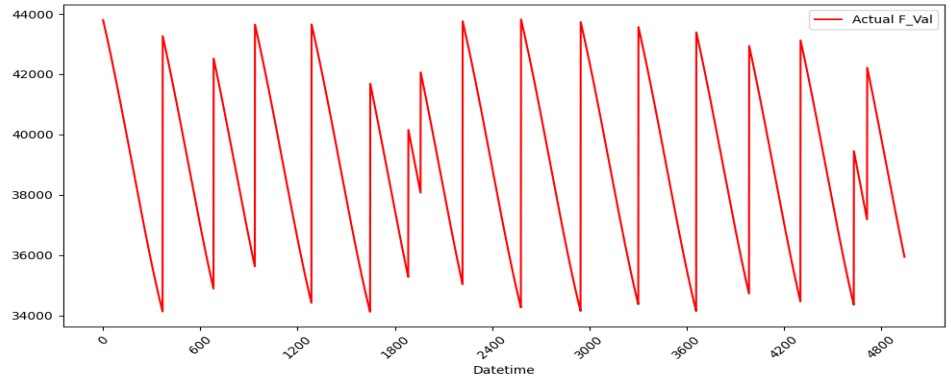


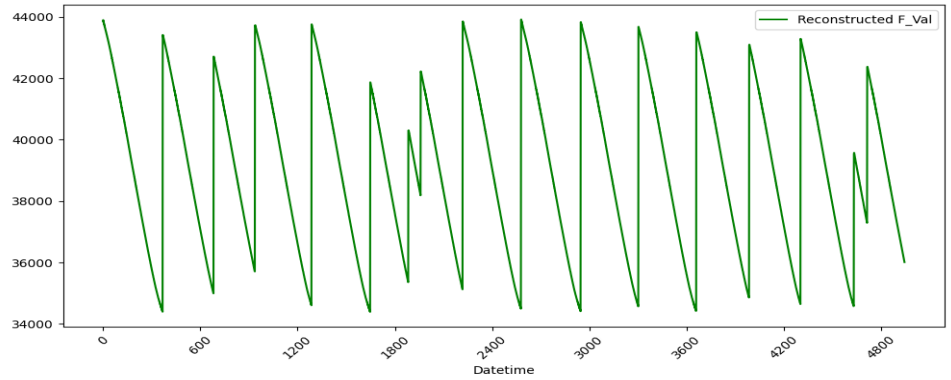


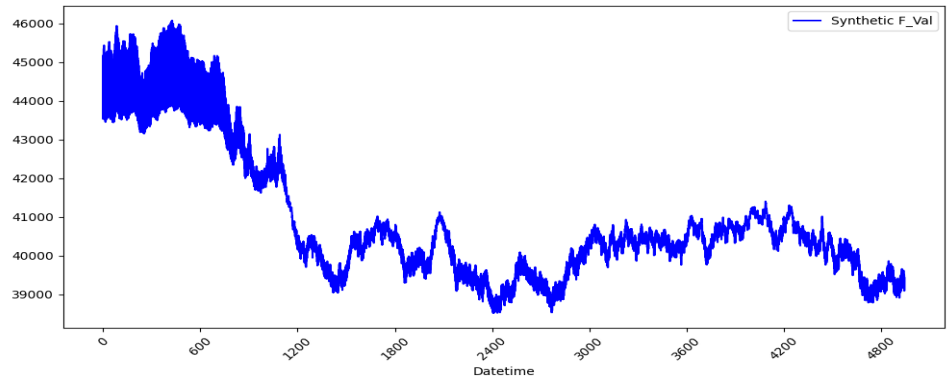


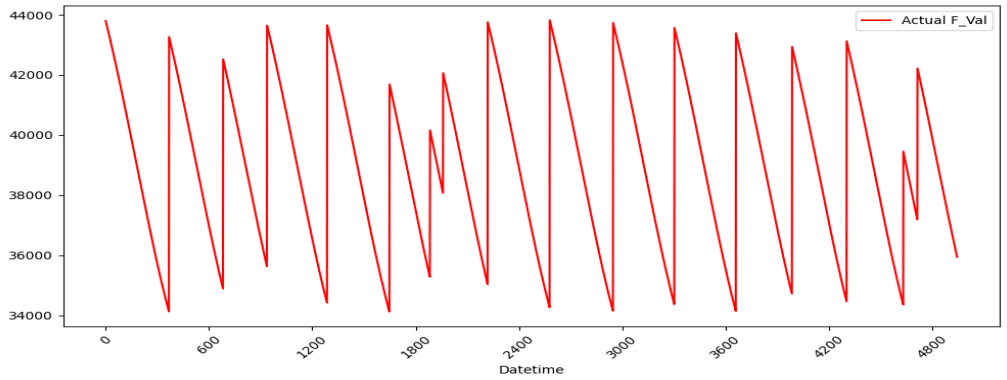


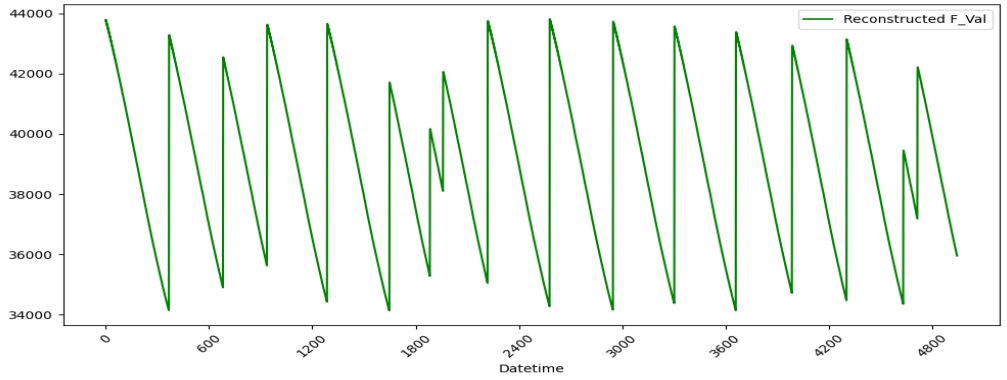
GAN for Synthetic Swarm Satellite Data

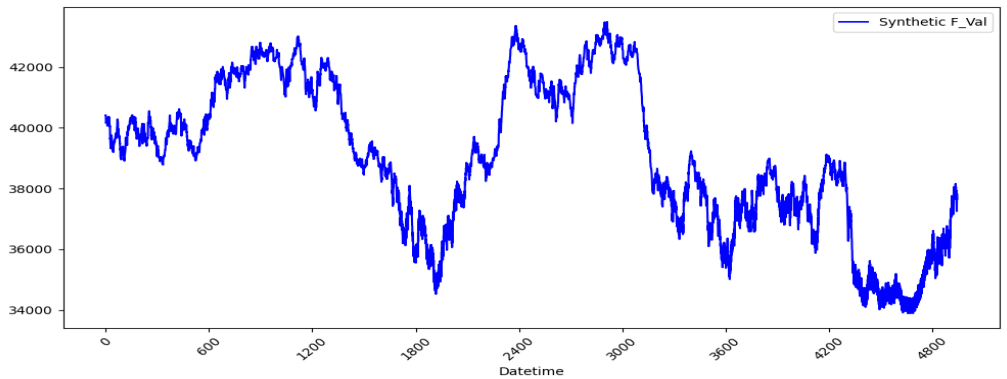




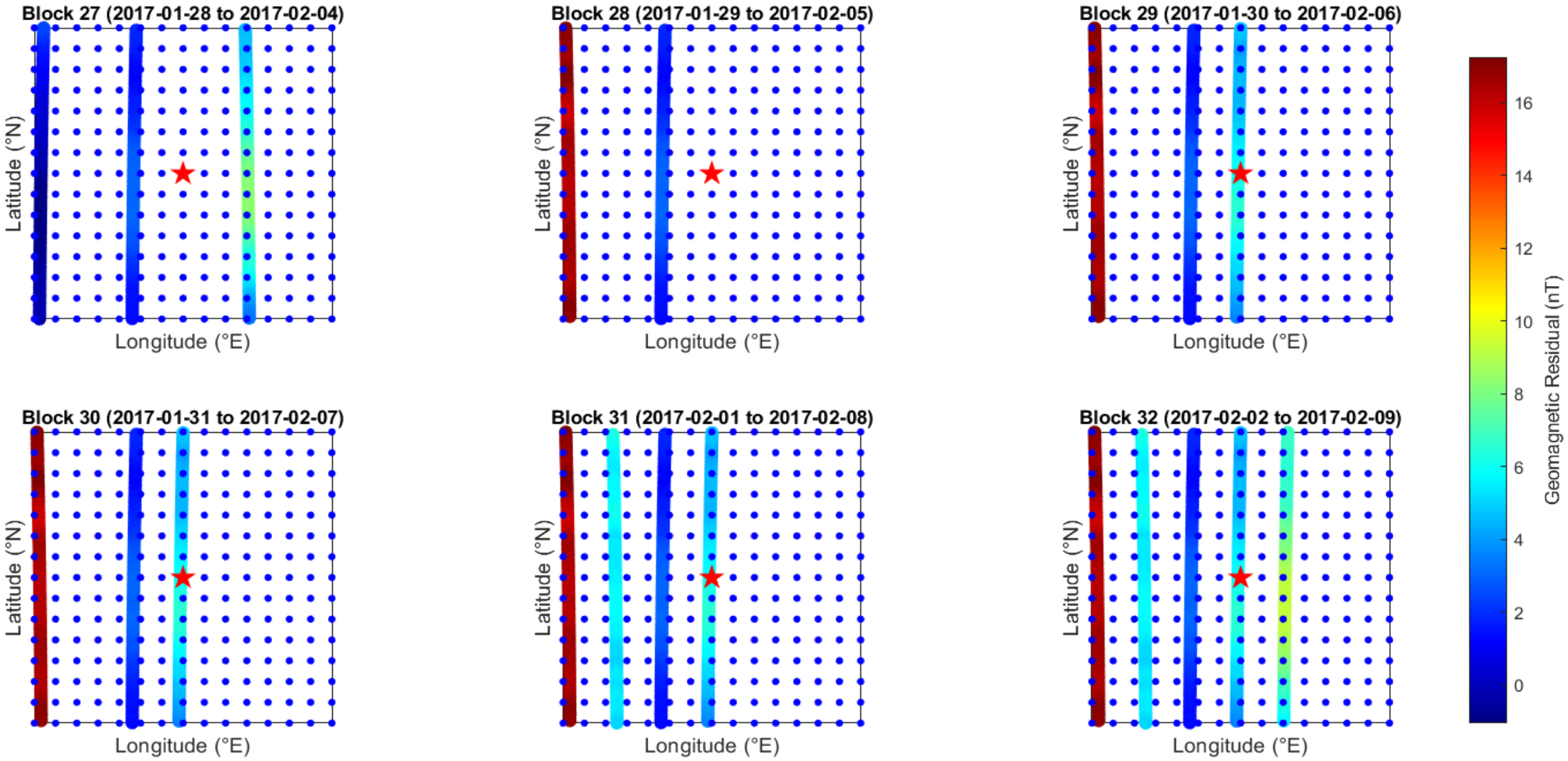




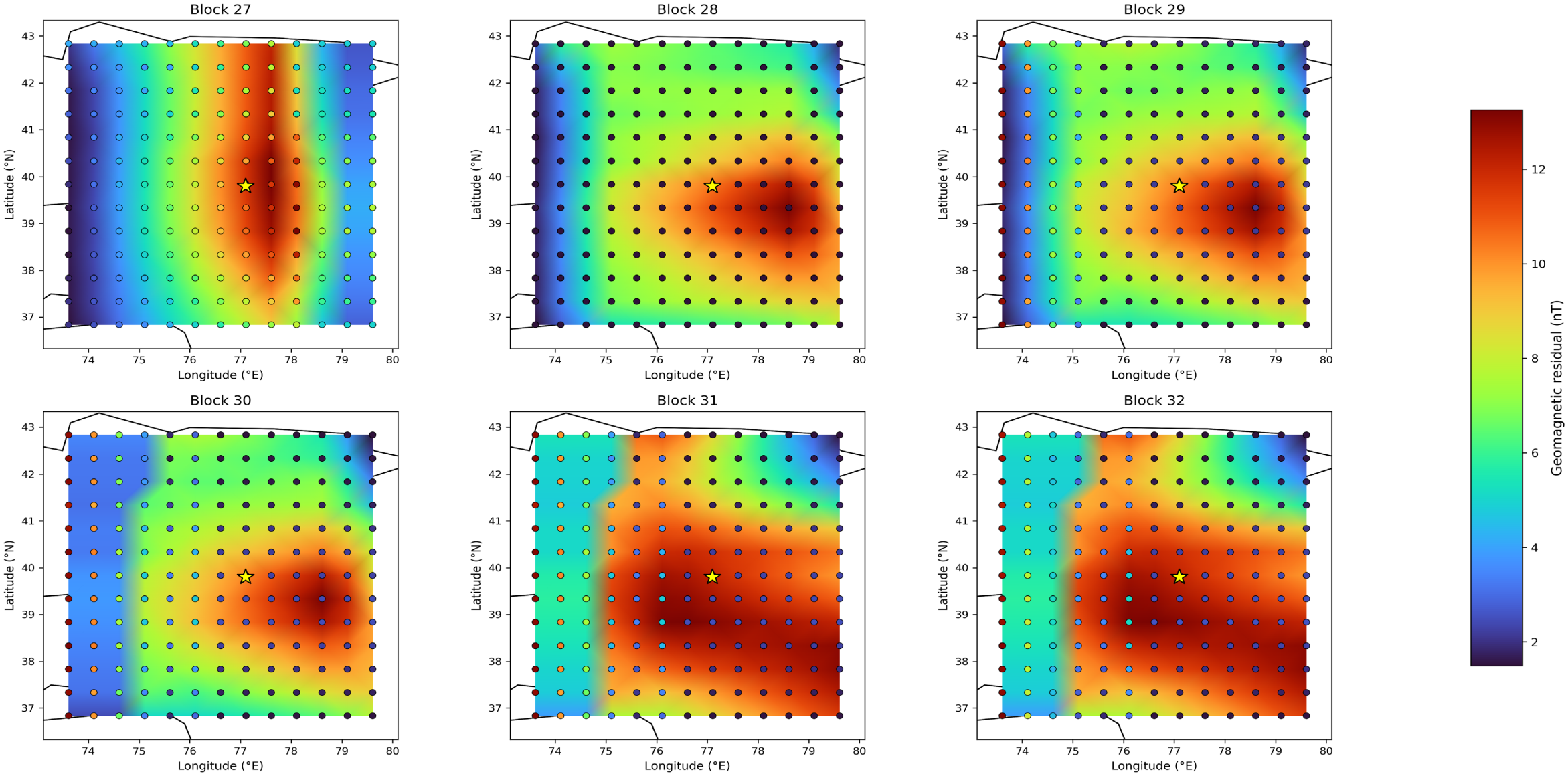




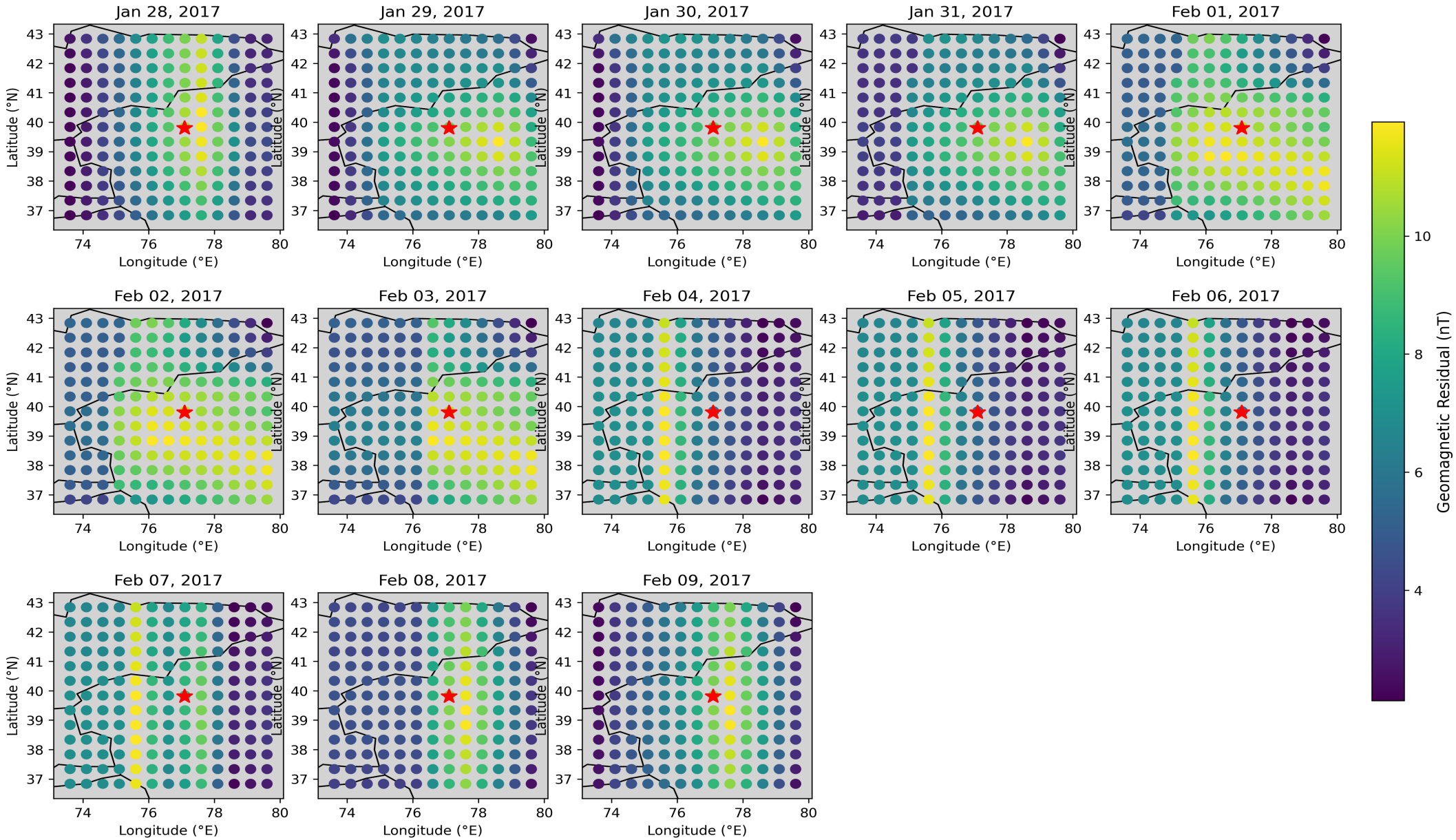
Blocks of 8-day Time Window Data Collected by the SWARM A and C between 28th July and 9th February 2017



Geomagnetic Residuals for 6 Generated Samples (6 blocks) using GAN

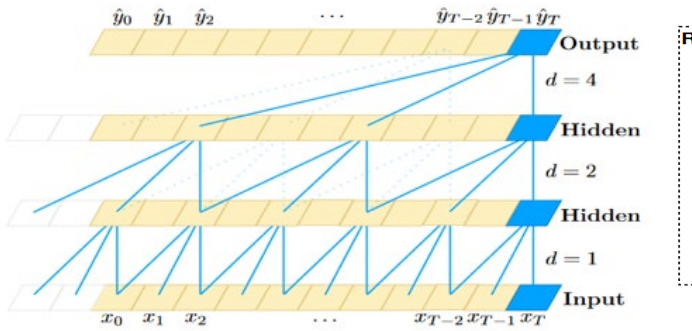


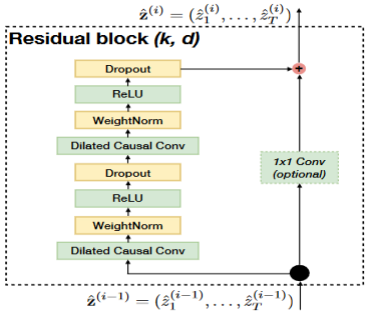
Geomagnetic Residual Data Generated within Blocks of 8 day Time Window

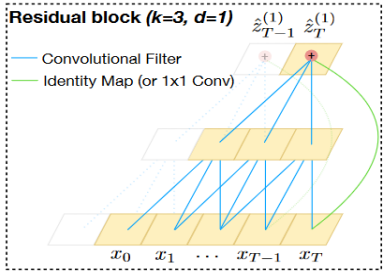


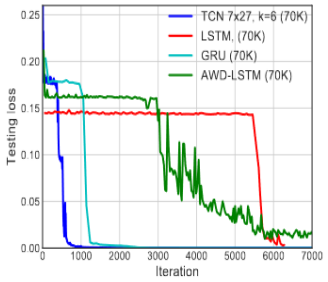
Part 3: TCN technology application on TEC modeling

Ionosphere Modeling and Prediction

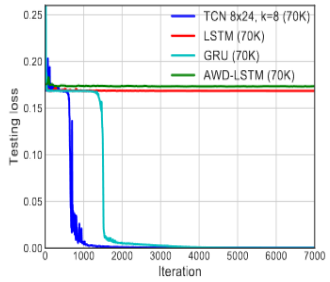




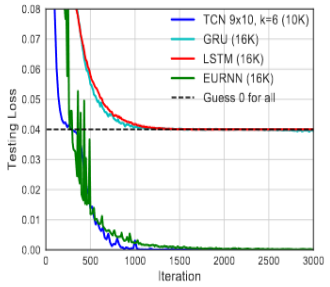




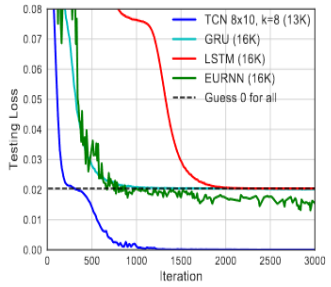
(a) $T = 200$



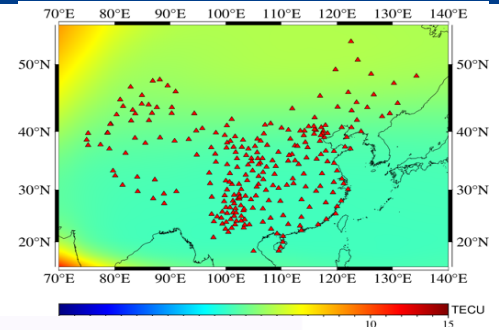
(b) $T = 600$

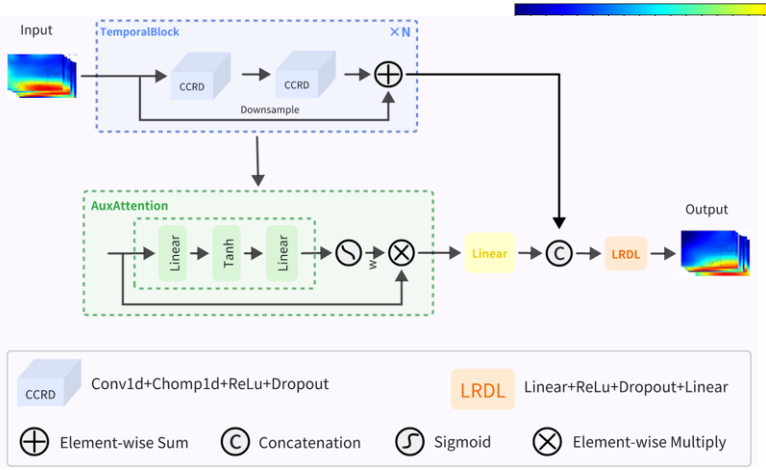


(a) $T = 500$



(b) $T = 1000$



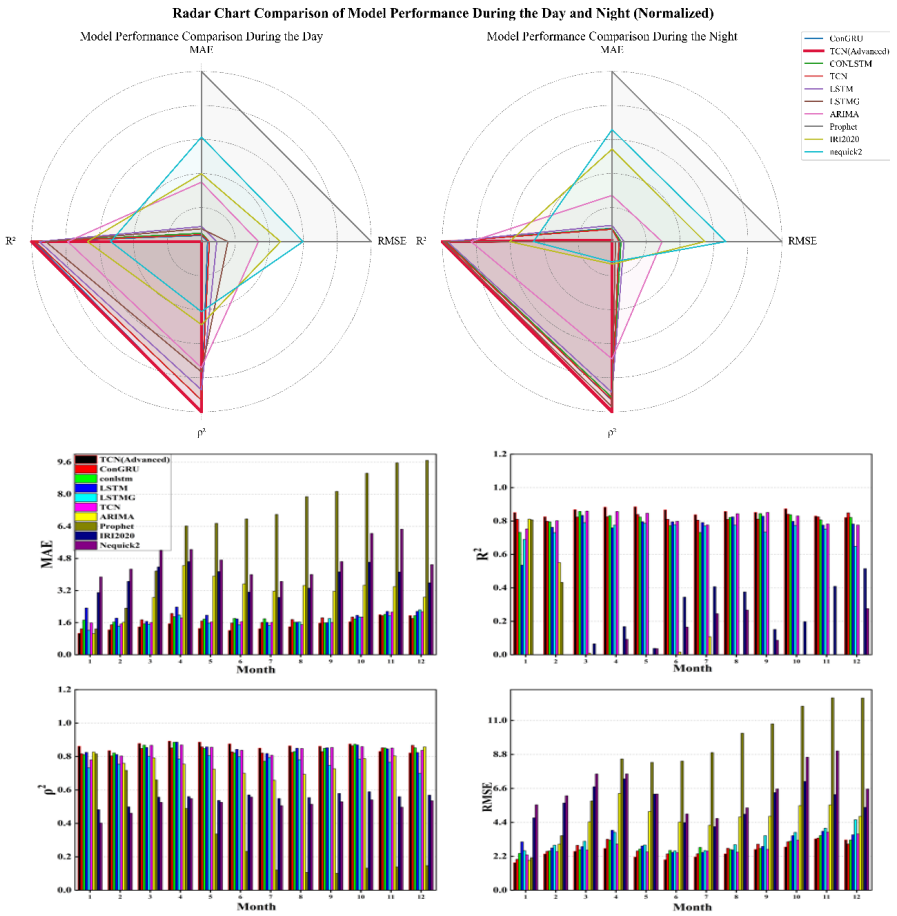


Explored AI-based methods for ionospheric prediction. By introducing a causal convolutional network and incorporating auxiliary data (e.g., solar activity, geomagnetic indices), an efficient and advanced deep learning model was constructed. Compared to existing deep learning models like ConvLSTM, our model achieves superior prediction accuracy and is approximately 10 times more computationally efficient.

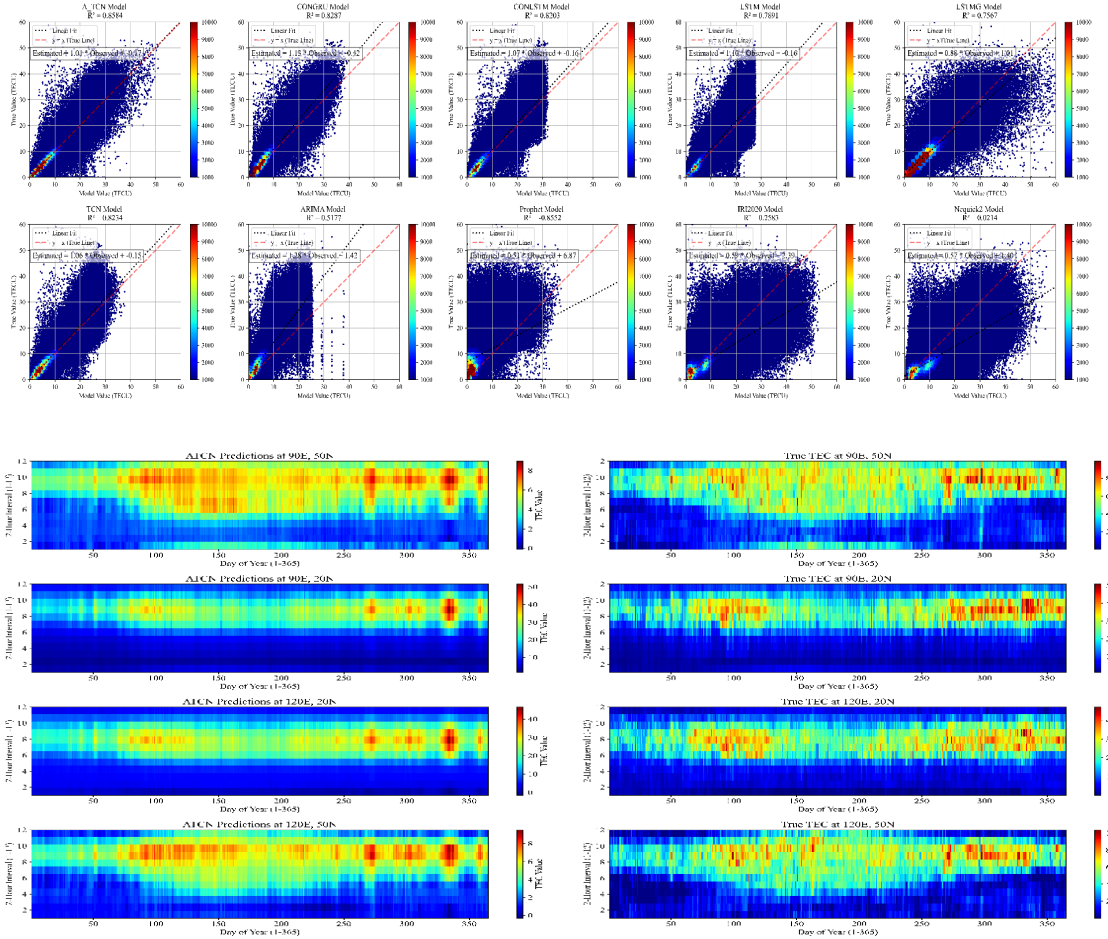
Chen et al., JGR, 2025

Part 3: TCN technology application on TEC modeling

Ionosphere Modeling and Prediction



Performance Comparison with 9 Benchmark Models (Statistical & ML Models)

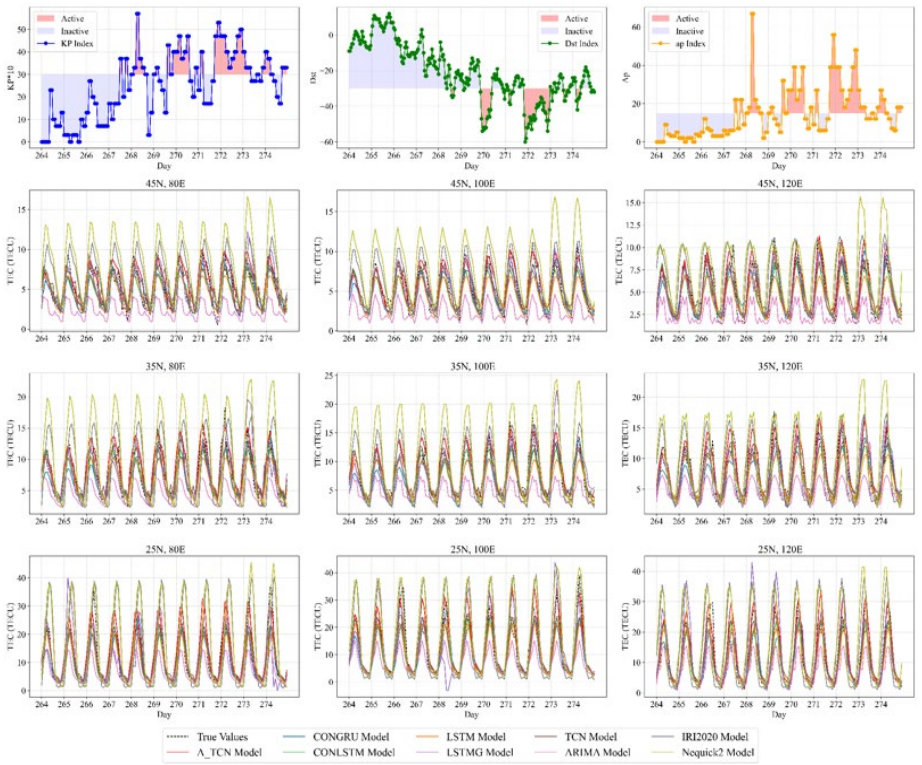


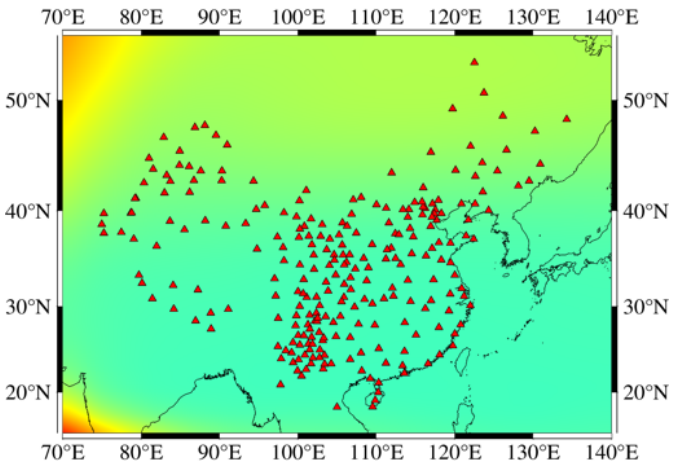
Overall, the model's performance surpasses the other 9 benchmarks, achieving higher prediction accuracy.

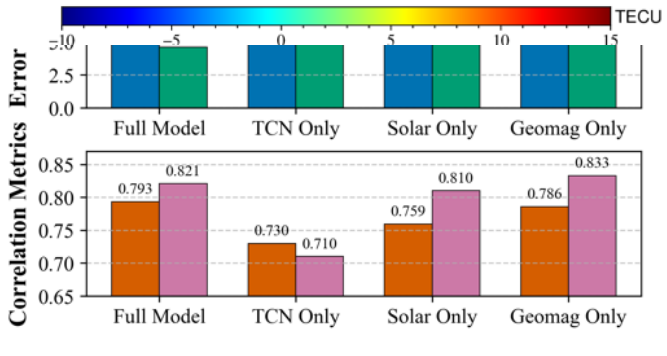
Chen et al., JGR, 2025

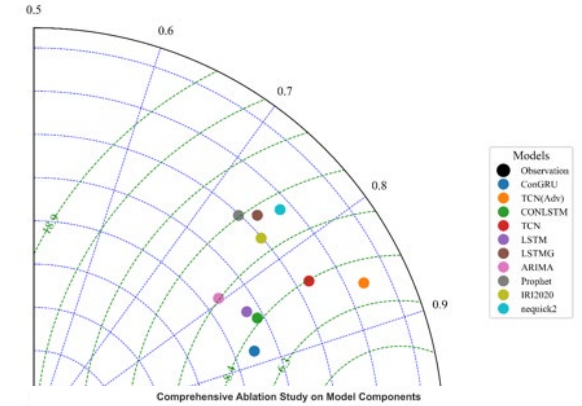
Part 3: TCN technology application on TEC modeling

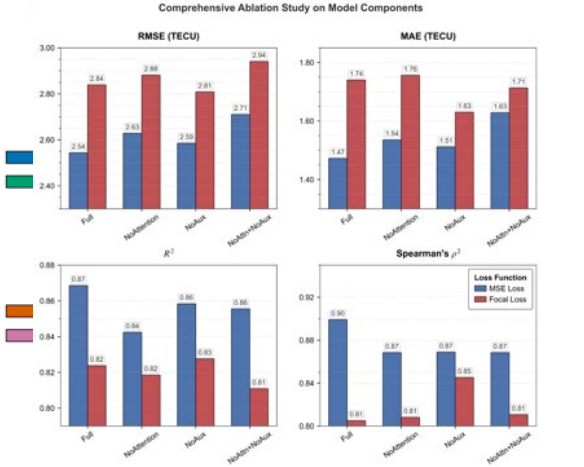
- **Ionosphere Modeling and Prediction**











During peaks of solar and geomagnetic activity, our model achieves superior prediction accuracy, demonstrating strong robustness.

JGR: Machine Learning and Computation, 2025

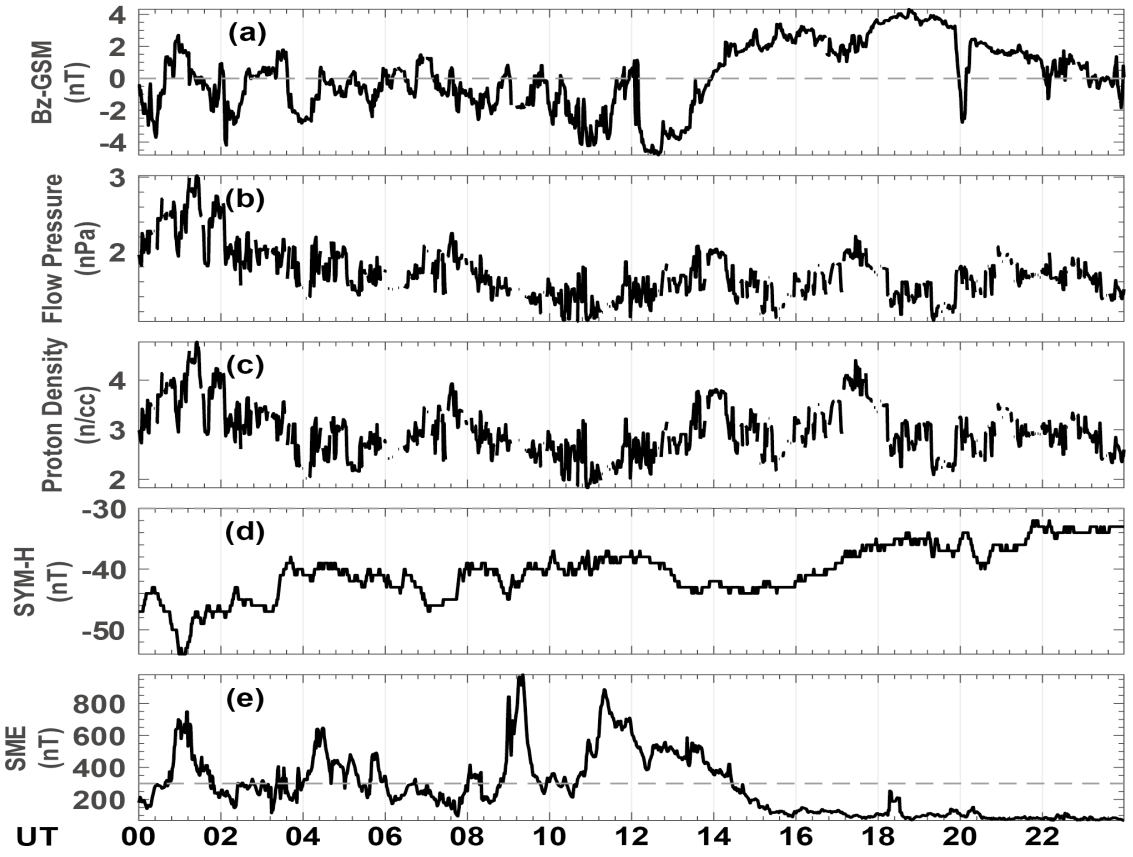
Part 4: EMIC waves during a geomagnetic storm

✓**EMIC waves:** Electromagnetic ion cyclotron waves in the Pc1 frequency range of 0.2–5 Hz, generated due to temperature anisotropy (T⊥>T∥) of energetic ions overlapping with cold, dense plasma.

✓Ionospheric EMIC wave frequency is different with local time

On August 28, 2018

- ✓ Several substorms between 00 and 14 UT
- ✓ During the recovery phase of a strong geomagnetic storm with the minimum Dst = −175 nT on August 26, 2018



Ouyang et al., JGR, 2024

Part 4: EMIC waves during a geomagnetic storm

EMIC waves in the ionosphere

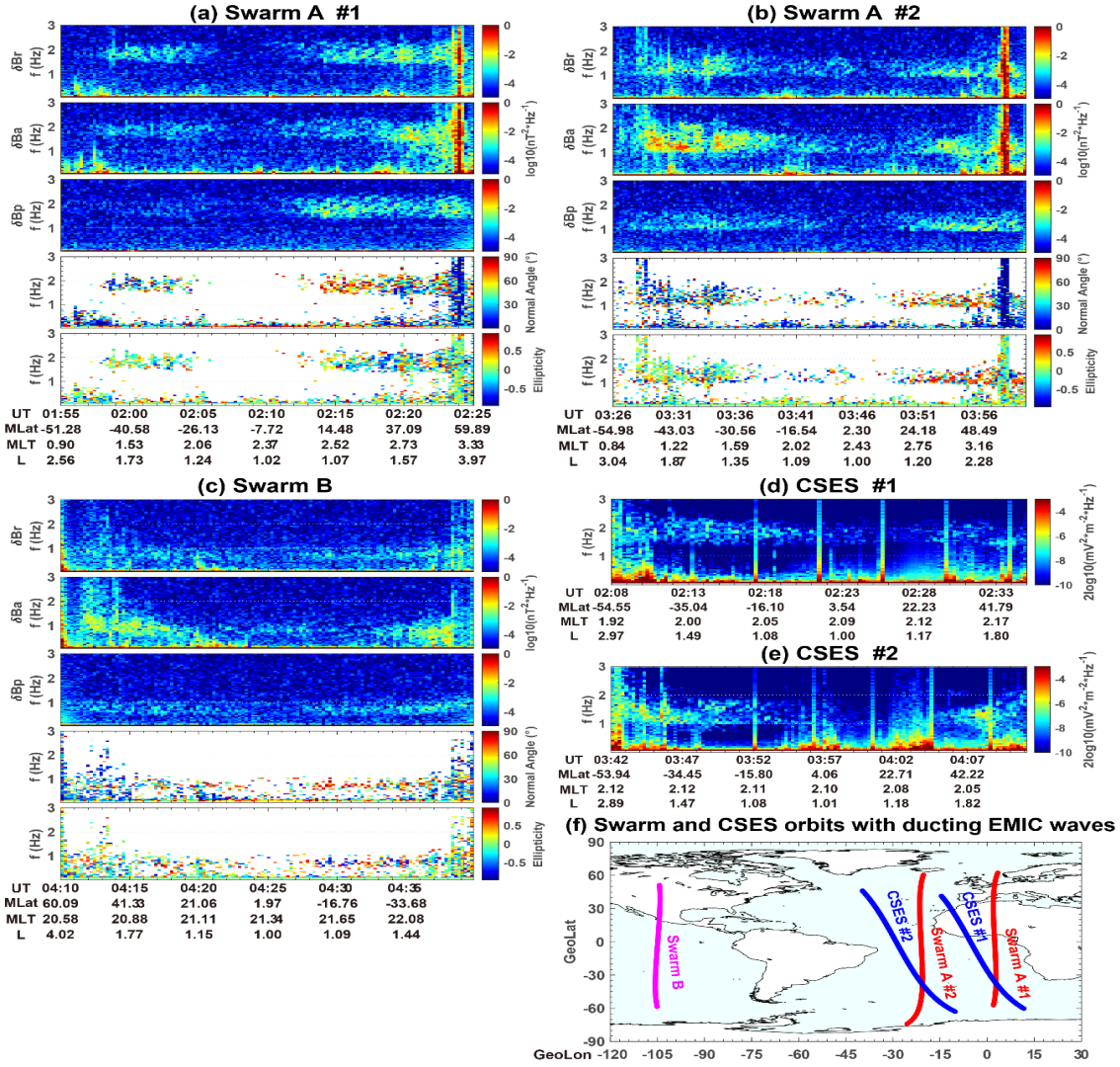
- Ducting EMIC waves were observed in the post- and pre-midnight sectors

In the post-midnight

- ✓ Swarm A observed EMIC waves starting from 01:57–02:25 UT (panel a), the other ducting waves were recorded during 03:26–04:00 UT (panel b)
- ✓ Two ducting EMIC waves were observed by CSES, which started at ~02 UT and continued to ~04 UT (panels d & e)

In the pre-midnight

- ✓ Swarm B observed ducting EMIC waves at ~ 04 UT (Panel c)



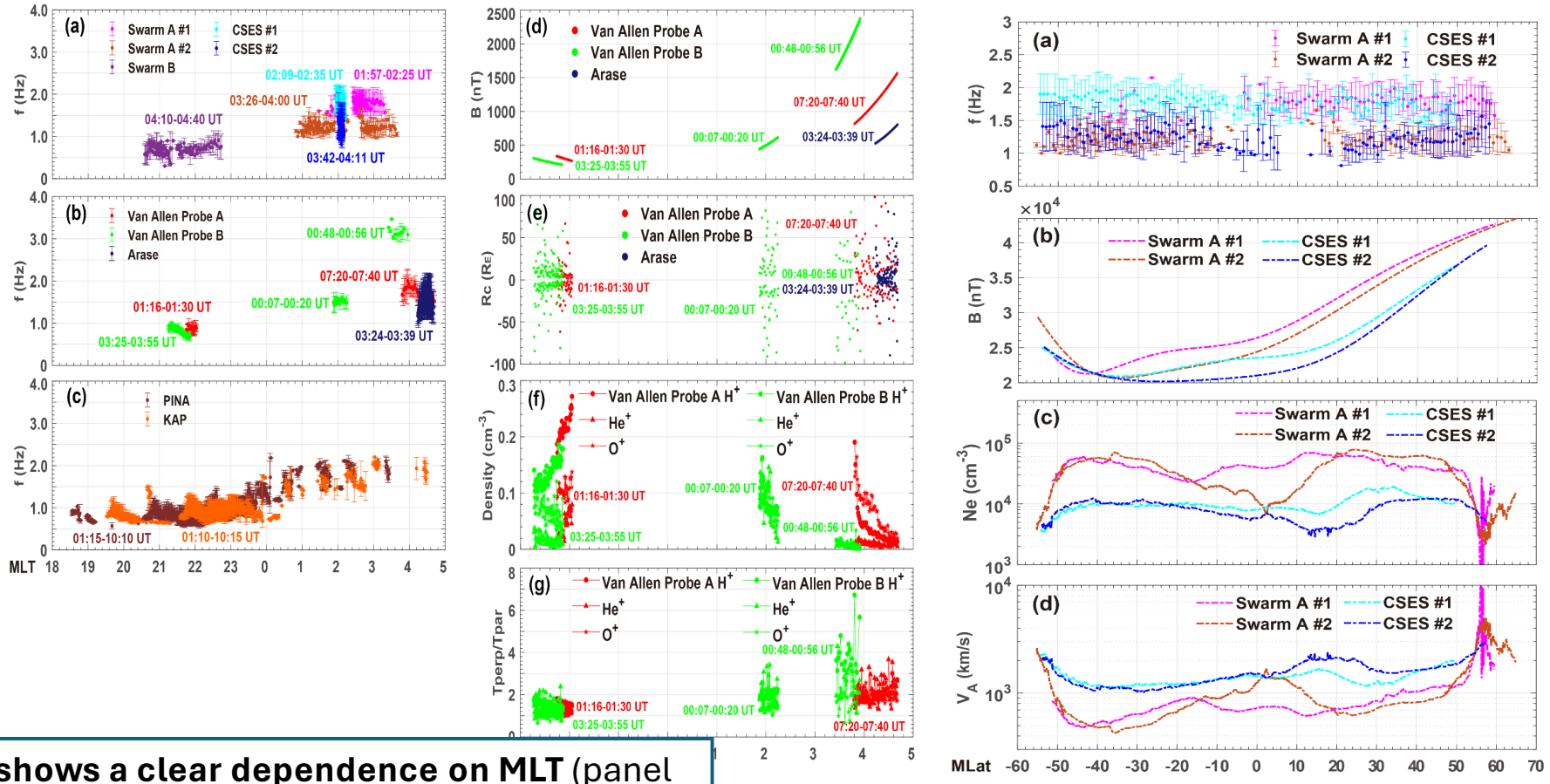
Ouyang et al., JGR, 2024

Part 4: EMIC waves during a geomagnetic storm

- EMIC waves in the ionosphere,magnetosphere and on the ground

(a-c): EMIC wave frequencies in the ionosphere, magnetosphere (He^+ band) and on the ground during the storm recovery phase on August 28, 2018

(d–g): Major parameters, including background magnetic field strength, magnetic field curvature radius, ion density and ion temperature anisotropy ($T_\perp/T_\parallel$) in the equatorial magnetosphere, that may affect EMIC wave generation and its frequency



Background magnetic field shows a clear dependence on MLT (panel d), whereas other parameters' change with MLT can be negligible

Ouyang et al., JGR, 2024

Part 5: Earthquake-related anomaly distinguishment

- 2023/12/18 Jishishan Ms6.2

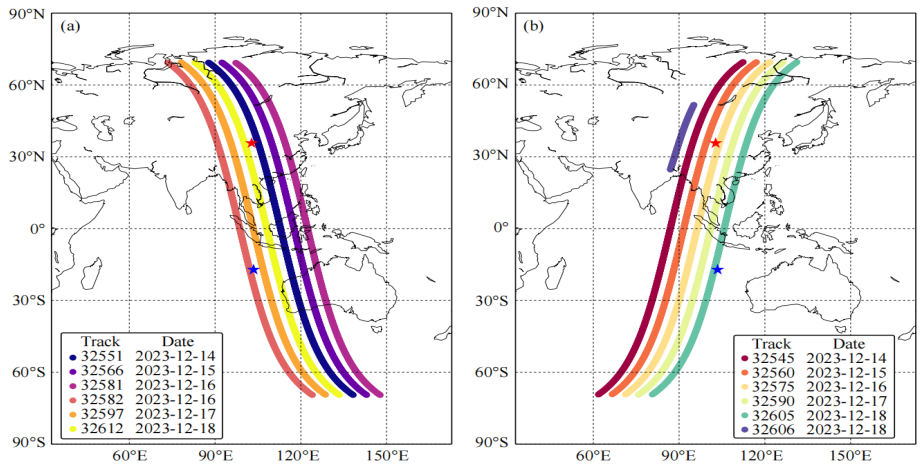
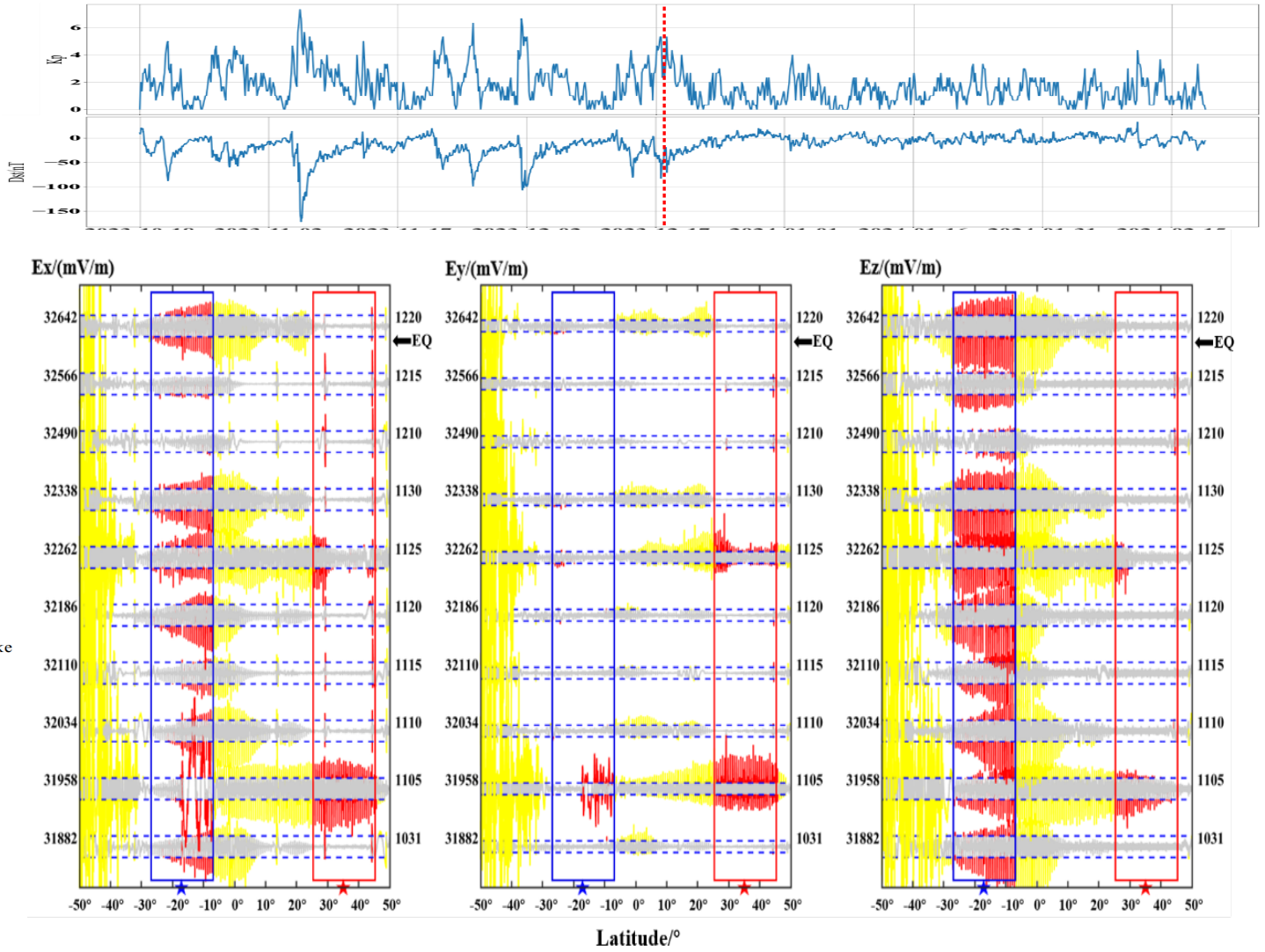


图 1　震前 5 天内的 (a) 夜间和 (b) 日间卫星轨迹投影图

红星代表震中，蓝星代表震中磁共轭点.

Fig. 1　The satellite trajectory projection maps of (a) nighttime and (b) daytime within 5 days before the earthquake

The red star represents the epicenter and the blue star represents the magnetic conjugate point of the epicenter.

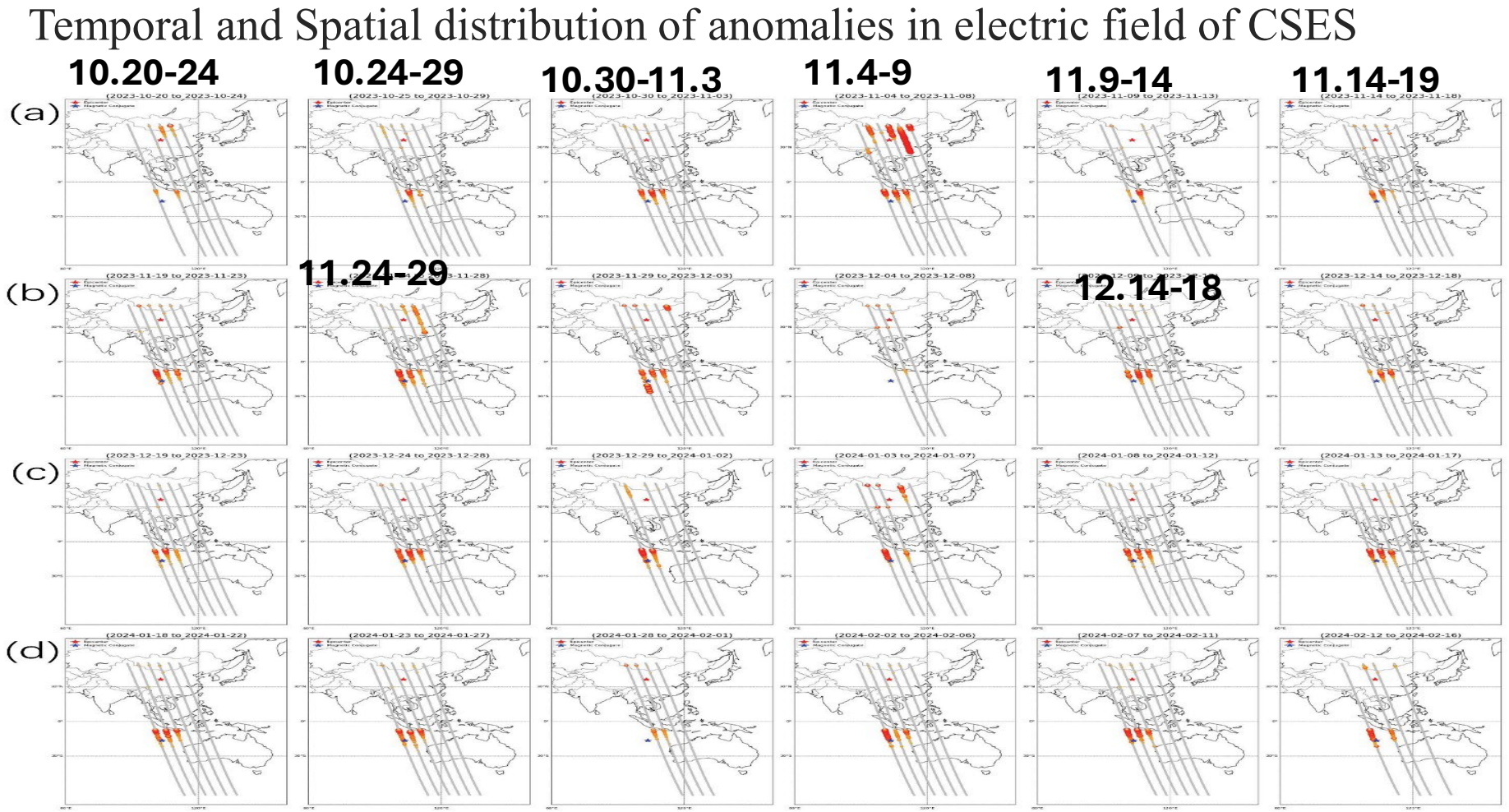


EMD analysis along the orbits during OCT 31 to DEC 20

Song et al., 2025

Part 5: Earthquake-related anomaly distinguishment

- 2023/12/18 Jishishan Ms6.2



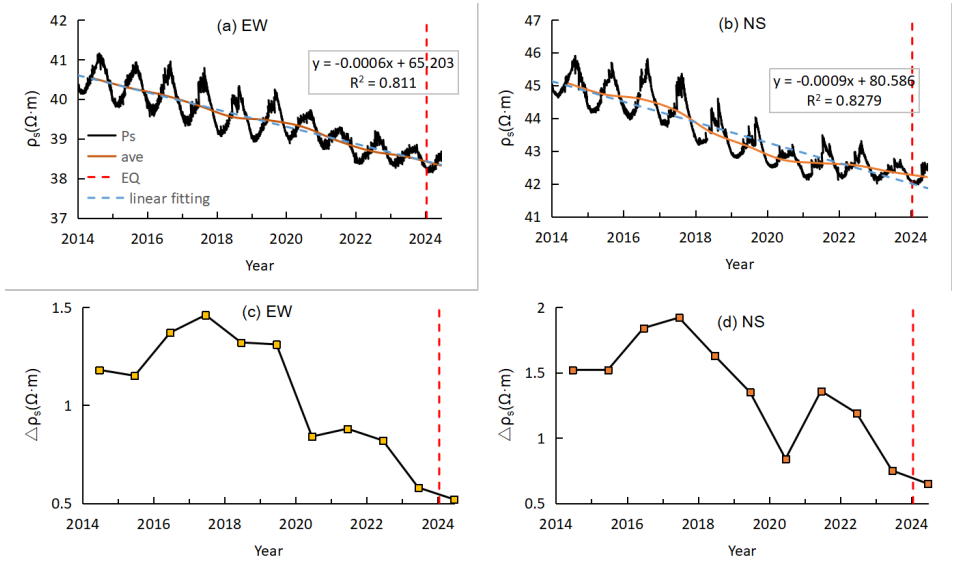
Song et al., 2025

Part 5: Earthquake-related anomaly distinguishment

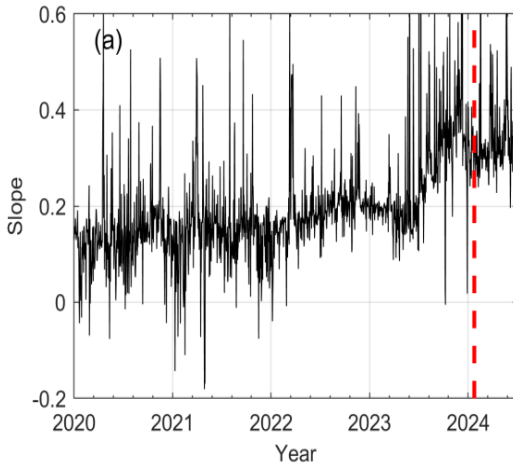
- 2024/01/22 Wushi Ms7.1

- Lithosphere

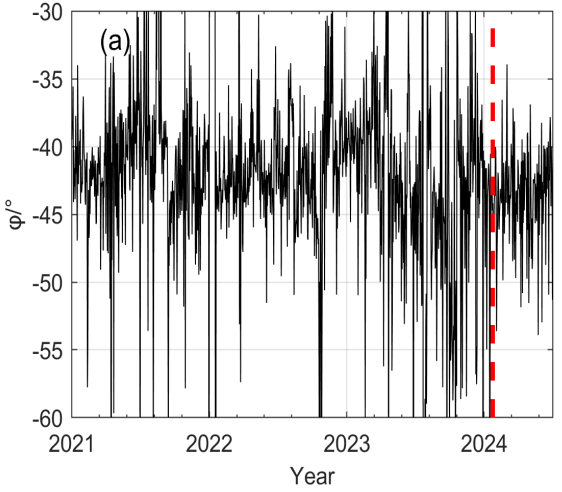
Earth resistivity at Keping station



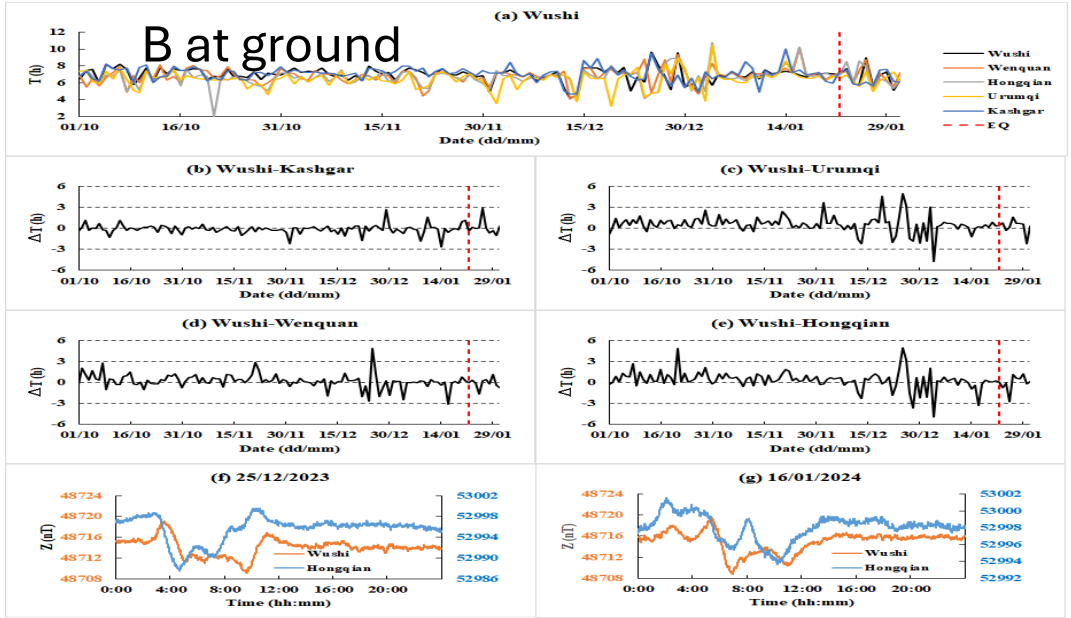
E at Wenquan



E at Wushi



B at ground



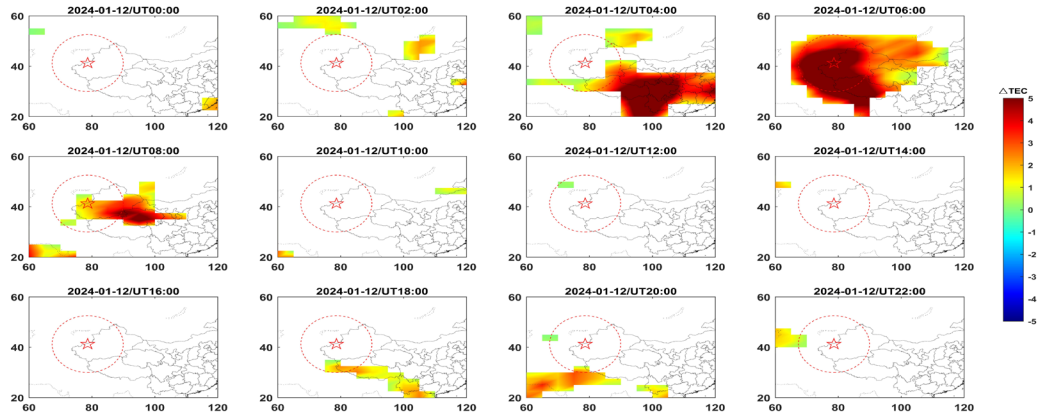
Zhang et al., 2025, JAES, under review

Part 5: Earthquake-related anomaly distinguishment

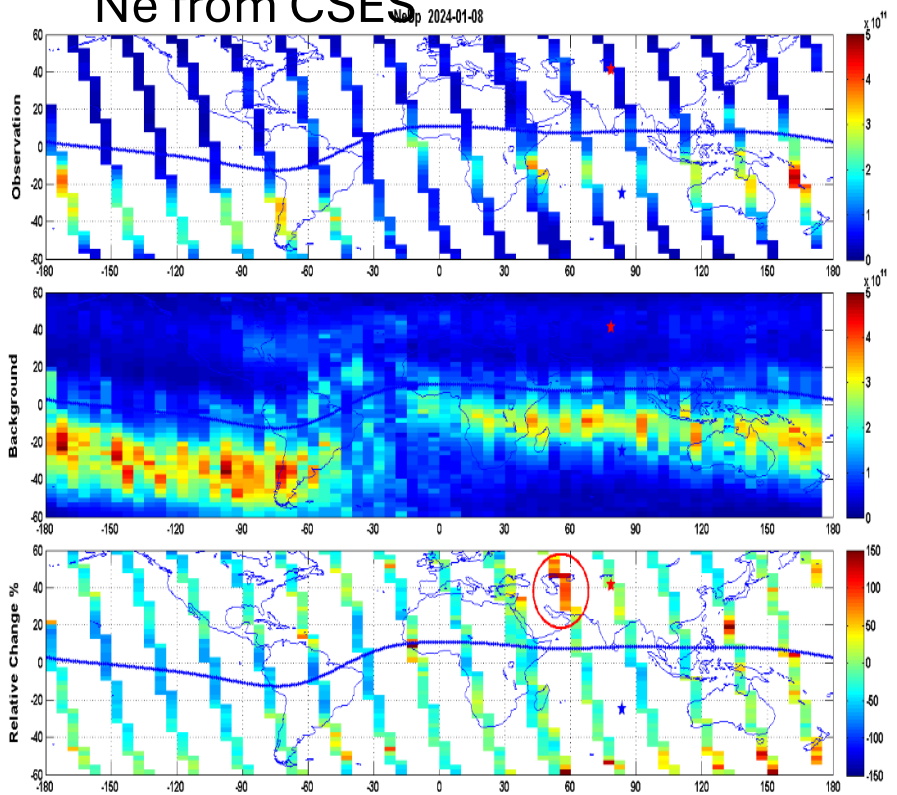
- 2024/01/22 Wushi Ms7.1

- Ionosphere

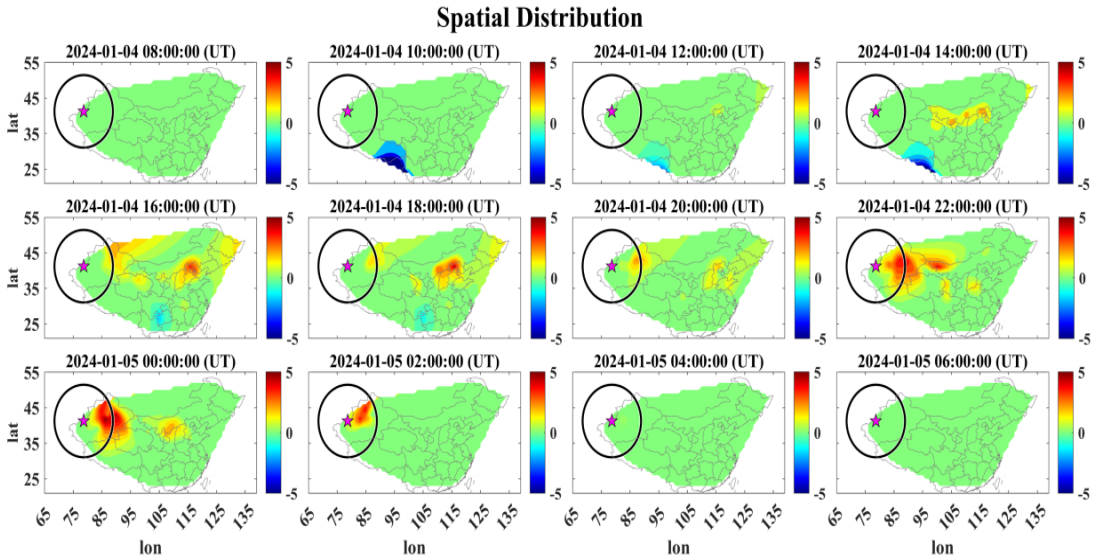
GIM TEC
CODE



Ne from CSES



GPS TEC



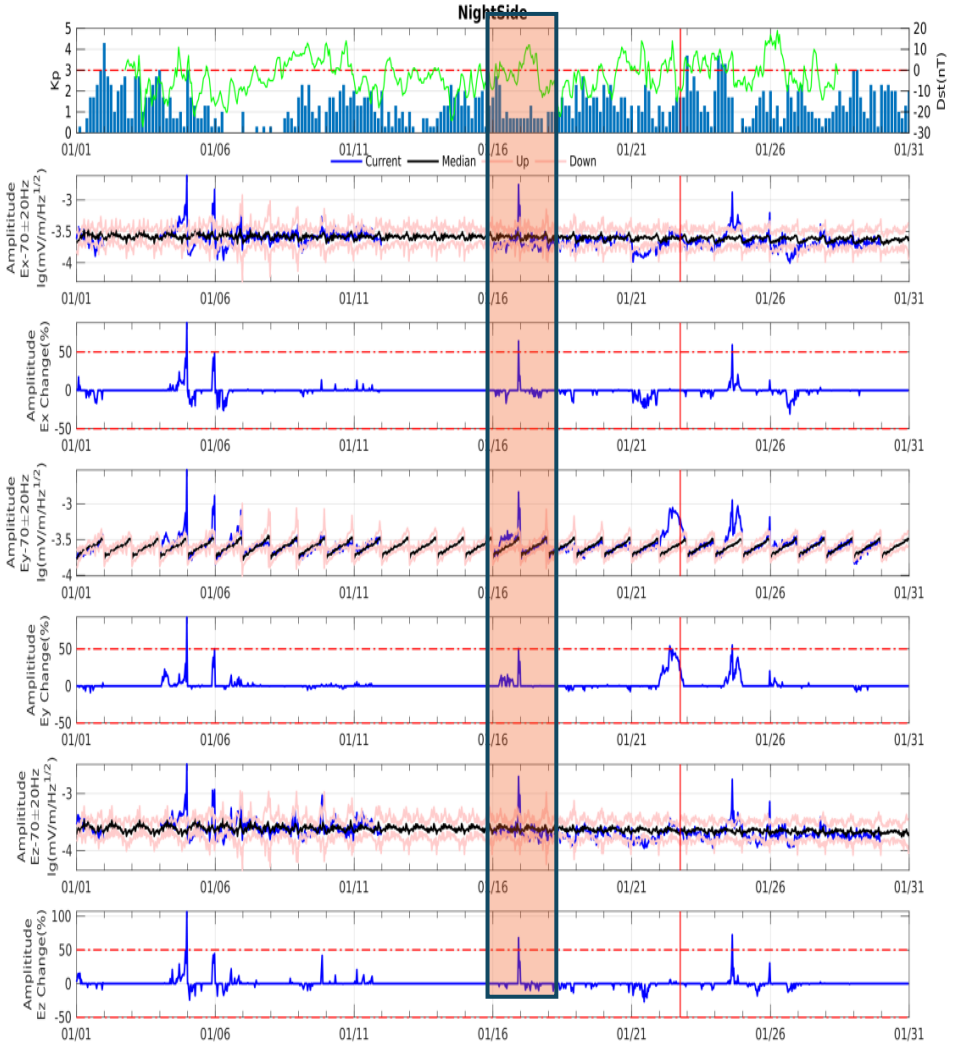
Zhang et al., 2025, JAES, under review

Part 5: Earthquake-related anomaly distinguishment

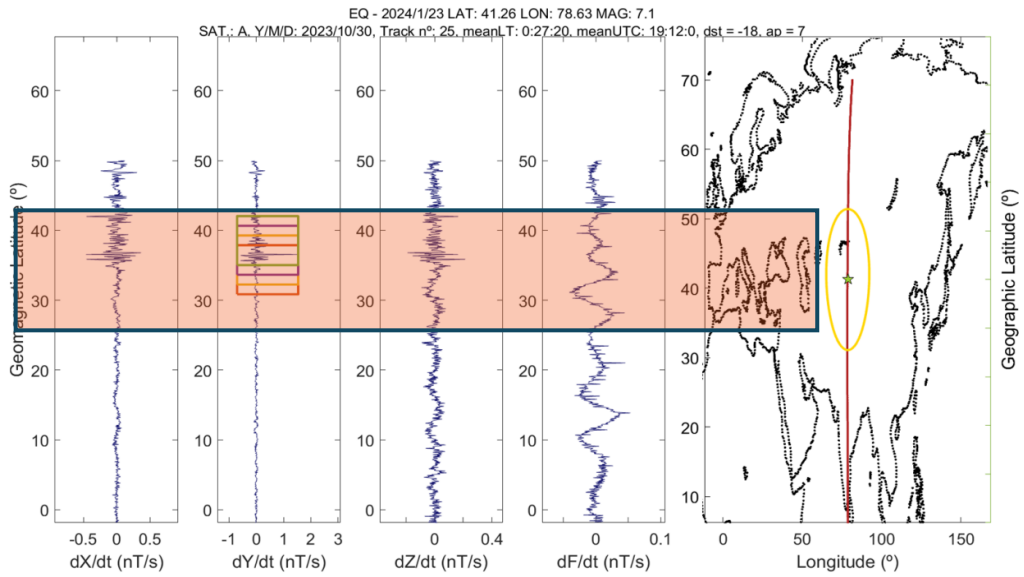
- 2024/01/22 Wushi Ms7.1

- Ionosphere

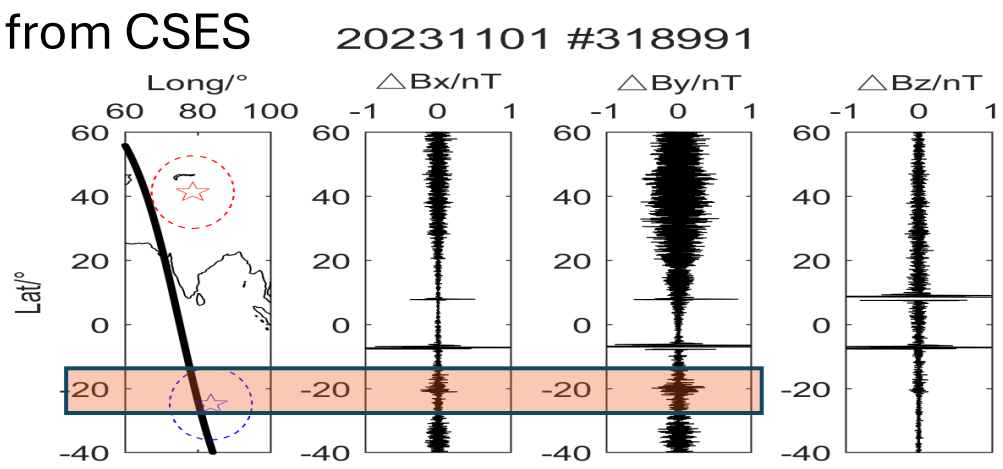
E from CSES



B from Swarm



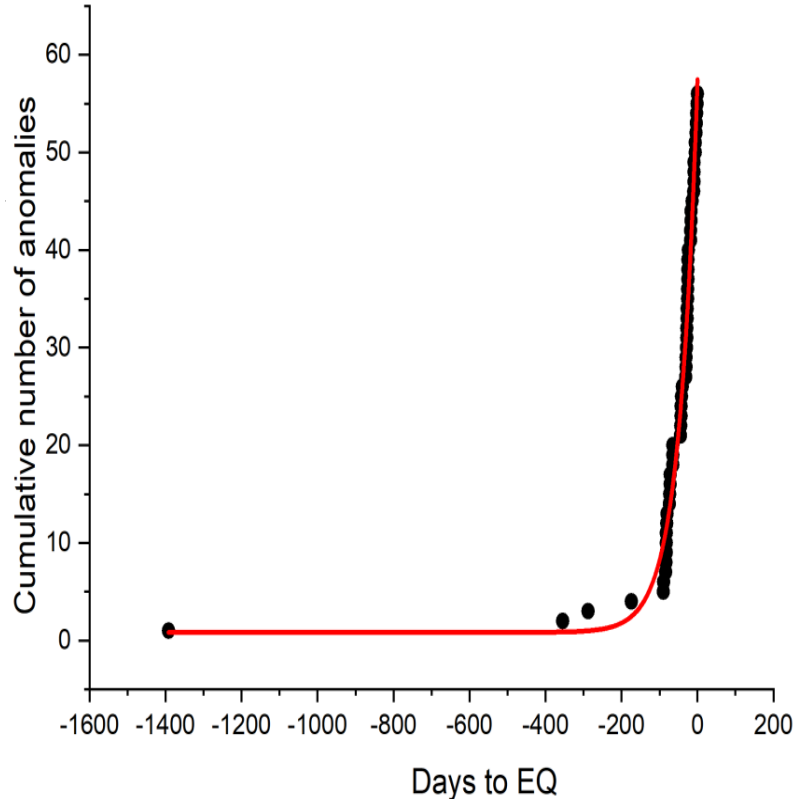
B from CSES

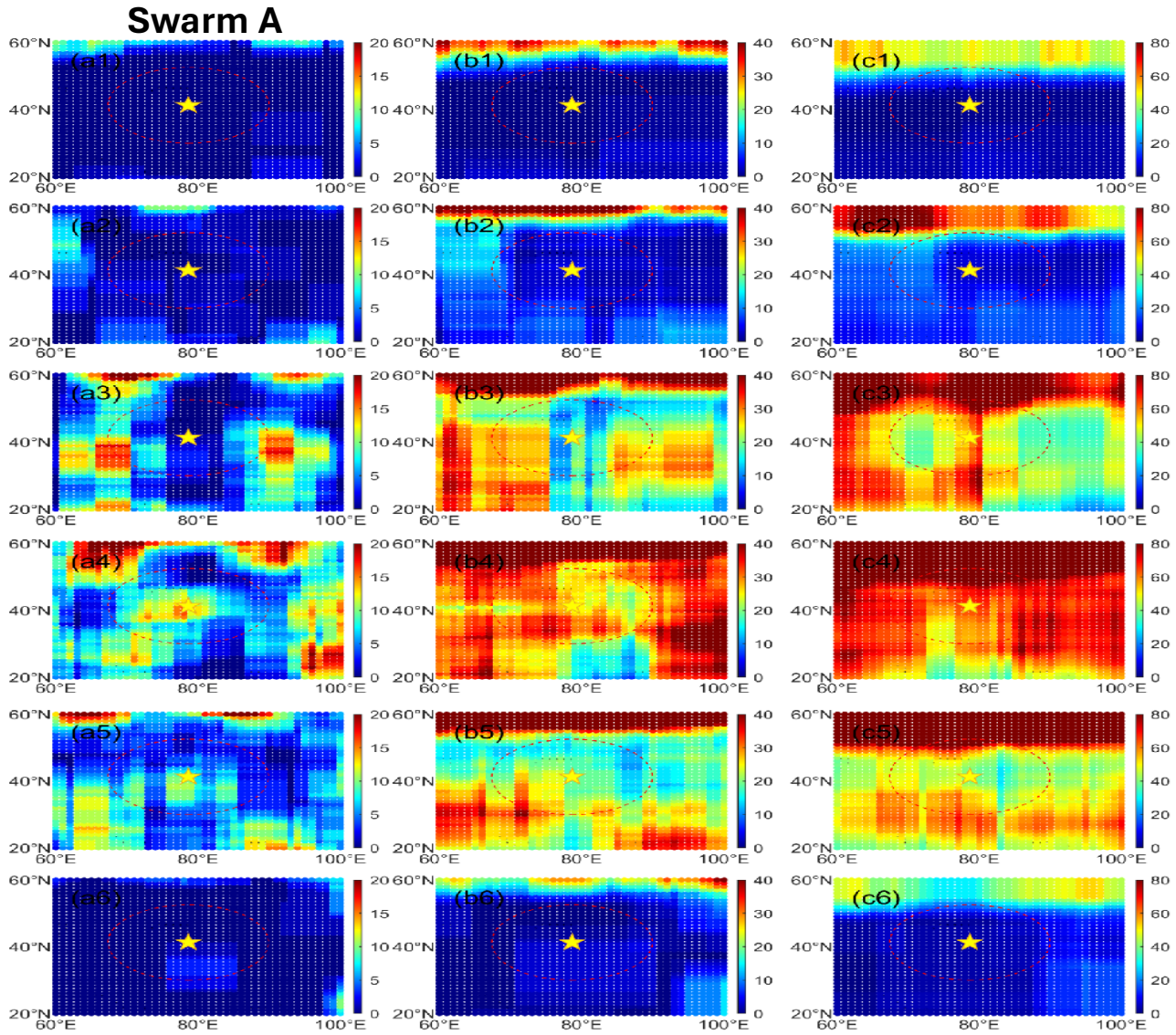


Zhang et al., 2025, JAES, under review

Part 5: Earthquake-related anomaly distinguishment

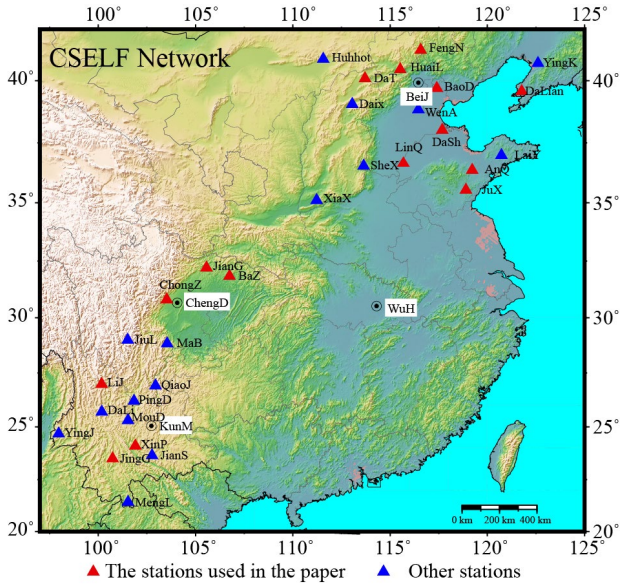
- 2024/01/22 Wushi Ms7.1

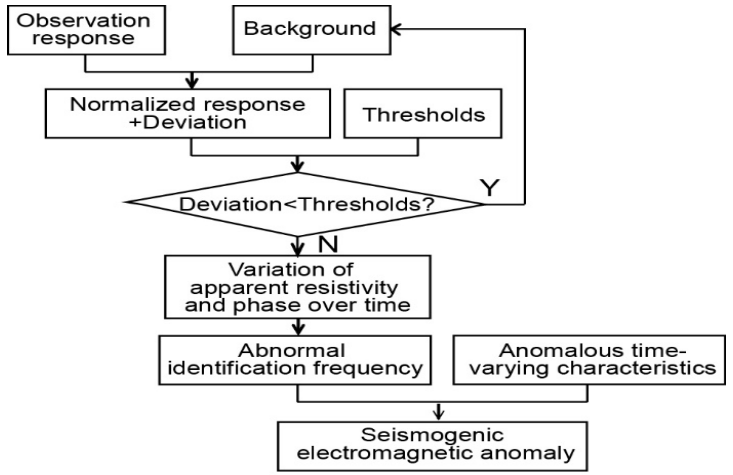




Zhang et al., 2025, JAES, under review

Part 5: Earthquake-related anomaly distinguishment

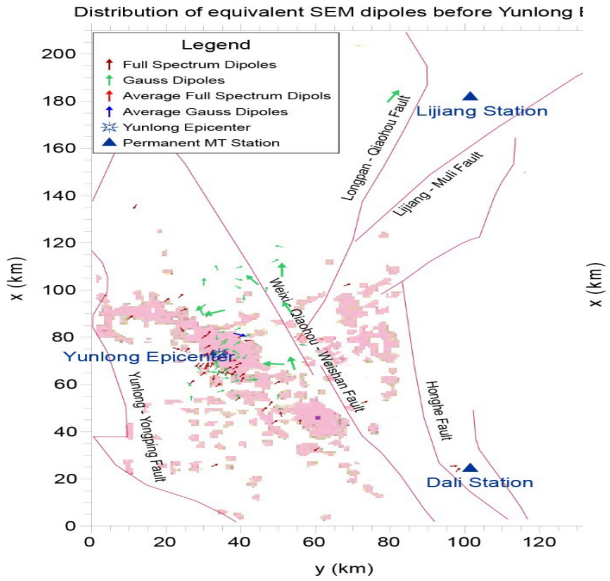


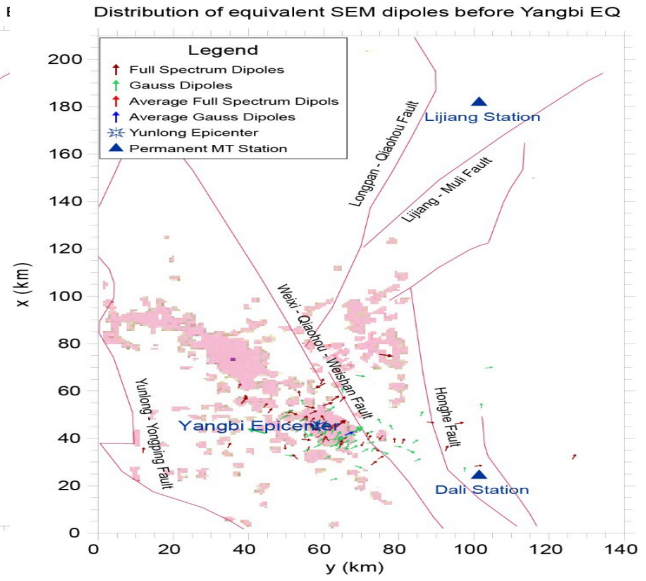




An **arbitrarily oriented electric dipole** at subsurface is used to simulate Seismogenic Electromagnetic (SEM) radiation emanating from a seismic zone during its gestation phase. Multiple parameters of dipole sources at subsurface were obtained by applying the **differential ant colony optimization (DACO) algorithm** to anomalous data of two stations with multi- frequencies and various response functions. The spatial distribution of these predicted dipoles is predominantly clustered in or around the seismogenic area, with their azimuthal orientation aligning towards the seismogenic fault in general.

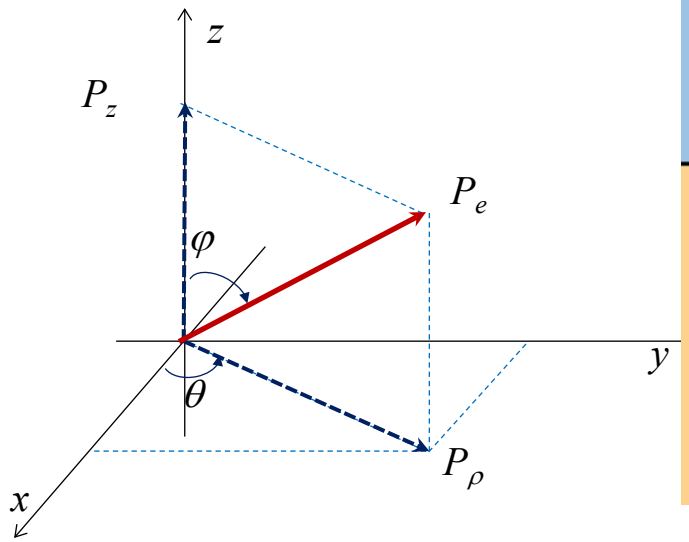
Han et al., 2024



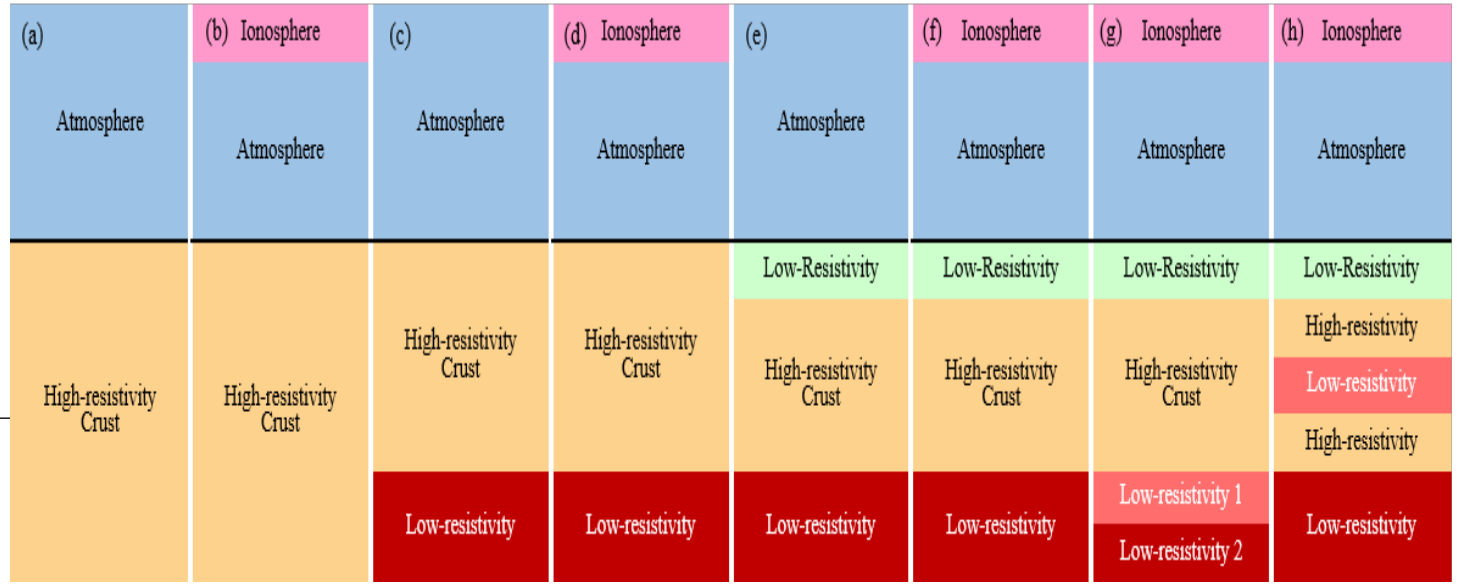


Part 5: Earthquake-related anomaly distinguishment

- **Eelctric dipole source and 2D layered Lithosphere-Atmosphere-Ionosphere models**



The seismic source as an electric dipole.

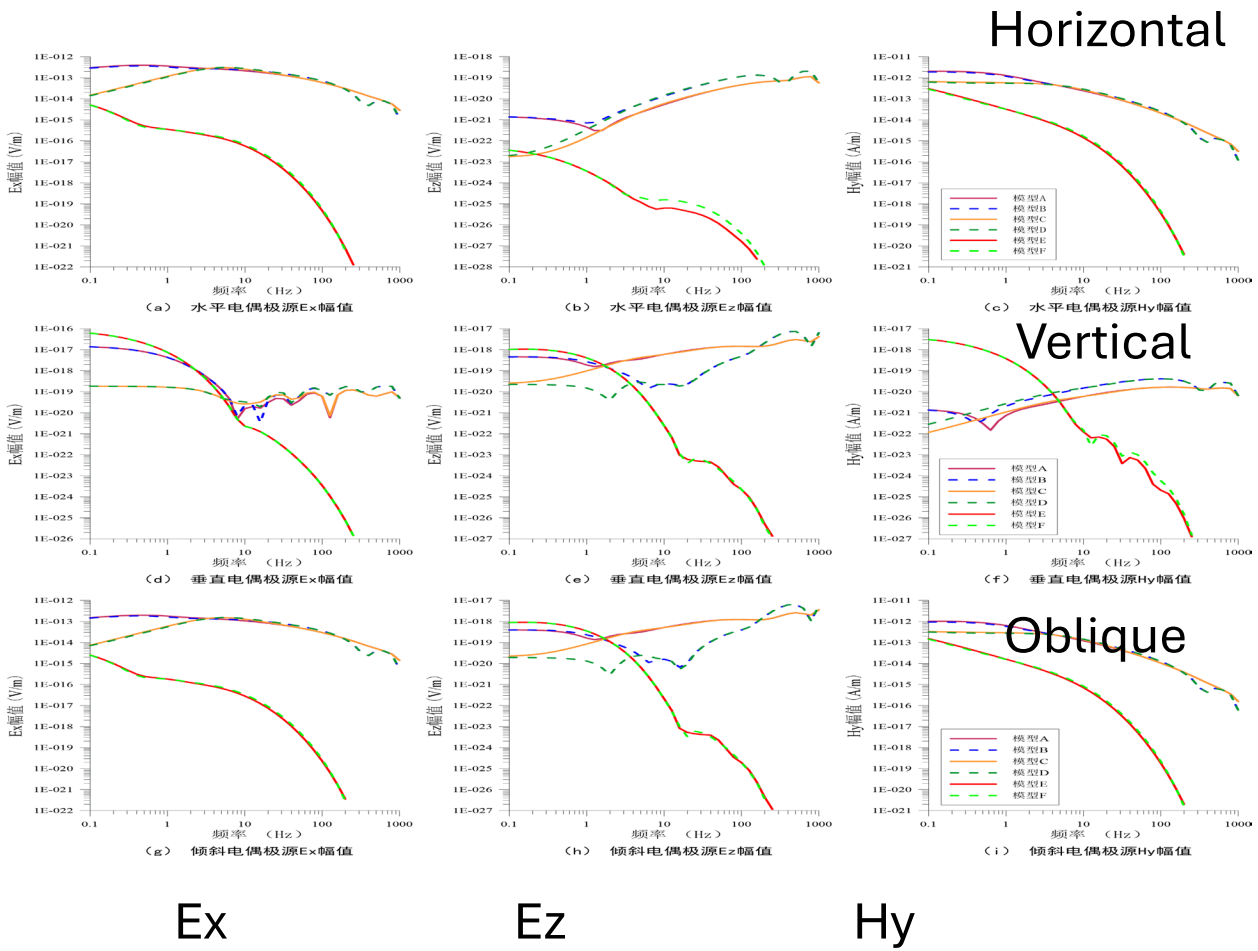


(a) Model A: uniform half-space earth model; (b) Model B: uniform half-space earth with the ionosphere above; (c) Model C: earth model with a lower crust conductive layer at depth; (d) Model D: earth model with the ionosphere above and a lower crust conductive layer at depth; (e) Model E: earth crust waveguide model; (f) Model F: earth crust waveguide - LAI waveguide model; (g) Model G: earth crust waveguide - LAI waveguide model with gradually increasing of lower crust conductivity; (h) Model G: earth crust waveguide - LAI waveguide model with a inner-crust conductive layer.

Wang et al., 2024

Part 5: Earthquake-related anomaly distinguishment

- **Eelctric dipole source and 2D layered Lithosphere-Atmosphere-Ionosphere models**
  - **Electromagnetic radiation in high-resistivity terrains exhibits slow attenuation** or even amplitude enhancement within both the crustal waveguide and the LAI waveguide; however, these two waveguide effects demonstrate distinct frequency selectivity;
  - **Within the high-resistivity media of the waveguides (specifically, the high-resistivity rock layers of the crustal waveguide and the atmosphere in the LAI waveguide), electromagnetic radiation is characterized by strong amplitude and slow attenuation.**
  - It is recommended to deploy monitoring stations:
    - a) On the surface where high-resistivity strata are exposed,
    - b) Within high-resistivity rock layers in boreholes or on the seafloor,
    - c) And within the atmosphere.
  - **The vertical field component exhibits more pronounced waveguide effects, making it particularly advantageous for long-distance detection.**



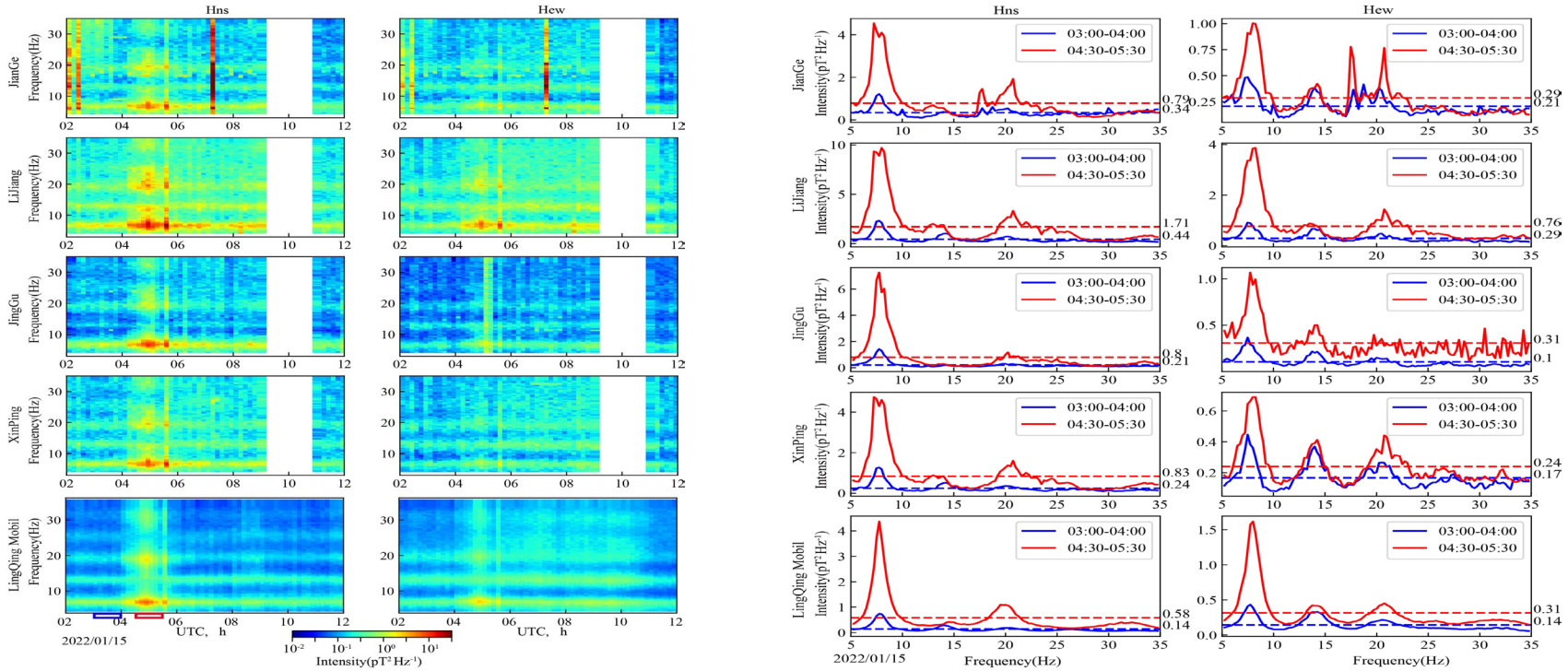
Wang et al., 2024

Part 6: Volcano effects on EM observations

- **Impact of the Hunga Tonga-Hunga Ha'apai volcanic eruption on Schumann Resonance**

The electromagnetic field intensity during the eruption period increased by approximately a factor of four

Electromagnetic intensity increased during eruption

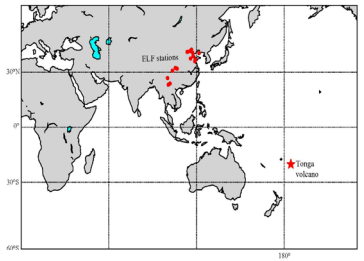


Power spectral intensity spectrograms observed during Tonga eruption (left) and spectra of calm and eruption periods(right)

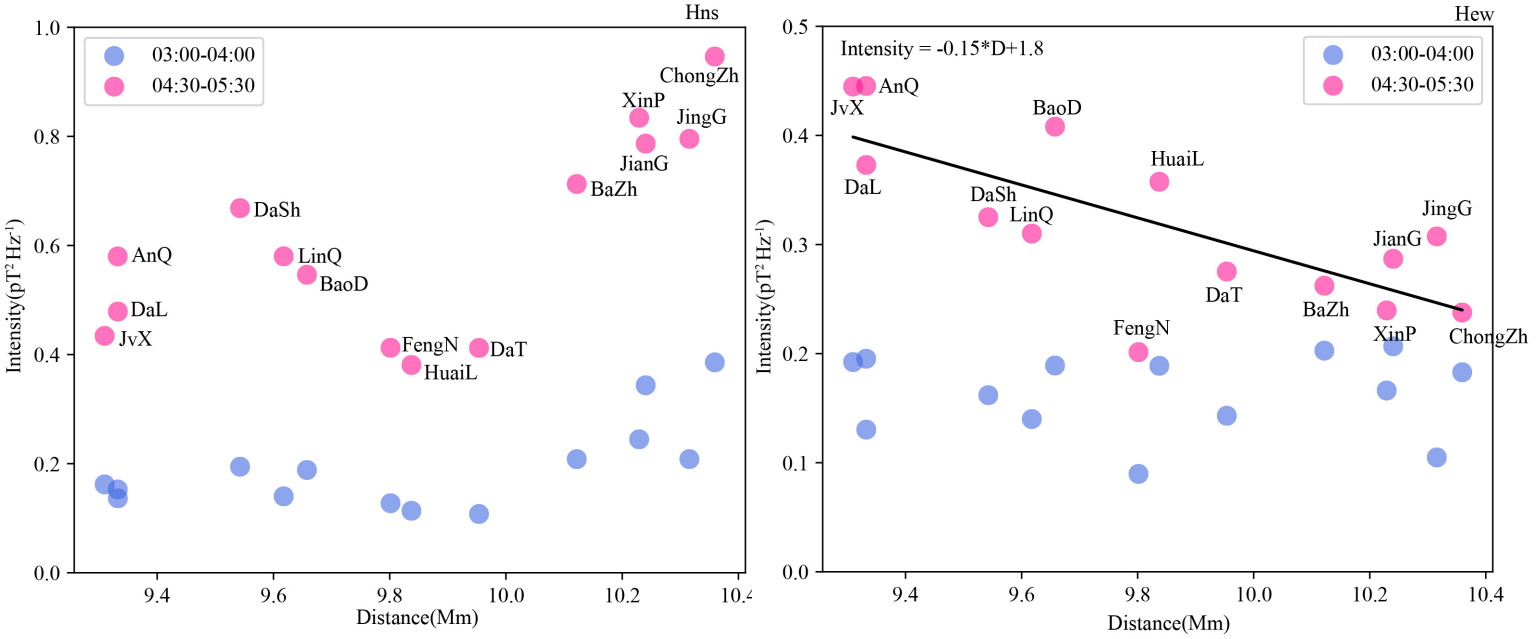
Han et al., 2025, under review

Part 6: Volcano effects on EM observations

- **Impact of the Hunga Tonga-Hunga Ha'apai volcanic eruption on Schumann Resonance**



The average intensity of during the quiet(blue) and eruption period(red), as well as their relationship with the distance from the volcano for each station:
For Hns, during the eruption period, both stations close to and far from the volcano experienced nearly the same times' significant enhancements



For Hew, during the eruption period, the intensity showed a tendency to weaken with increasing distance from the eruption center. represented by the equation: Intensity = -0.15×D + 1.8.

Han et al., 2025, under review

Summary

- AI methods like LSTM， GAN， TCN etc, has been developed to construct the global geomagnetic field and regional TEC map, the accuracy has been improved a lot.

- Multi methods have been used in electromagnetic anomaly detection during geomagnetic storm, EQs and Volcano, including, STL, EMD etc.

- The LAIC model has been developed within the frequency of 0.1-1000Hz to illustrate the long distance propagation for high resistivity terrains .



CSTEC
中国科学技术交流中心
China Science and Technology Exchange Center

esa
THE EUROPEAN SPACE AGENCY

Thank you very much for your attention!

Questions?